Anatomy and relationships of the bizarre Early Cretaceous pliosaurid *Luskhan itilensis*

Valentin Fischer[1,*], Roger B. J. Benson[2], Nikolay G. Zverkov[3], Maxim S. Arkhangelsky[4,5], Ilya M. Stenshin[6], Gleb N. Uspensky[7], Natalya E. Prilepskaya[8]

[1]Evolution & Diversity Dynamics Lab, Université de Liège, 14 Allée du 6 Août, Liège 4000, Belgium.
[2]Department of Earth Sciences, University of Oxford, South Parks Road, Oxford OX1 3AN, UK.
[3]Geological Institute of the Russian Academy of Sciences, Pyzhevsky Lane 7, Moscow 119017, Russia.
[4]Department of General Geology and Minerals, Saratov State University, A83 Astrakhanskaya Street, 410012 Saratov, Russia.
[5]Department of Geoecology and Engineering Geology, Saratov State Technical University, 77 Politekhnicheskaya Street, 410054 Saratov, Russia.
[6]Undory Paleontological Museum, Shkol'naya Ulitsa, 5, Undory, Ulyanovsk Oblast, 433340, Russia.
[7]Natural Science Museum, Ulyanovsk State University, Leo Tolstoy Street, Ulyanovsk 432000, Russia.
[8]Severtsov Institute of Ecology and Evolution of the Russian Academy of Sciences, 34 Vavilova Street, Moscow 119334, Russia.

*corresponding author: v.fischer@uliege.be

ABSTRACT

Pliosaurid plesiosaurians are iconic marine reptiles that regulated marine trophic chains from the Middle Jurassic to the early Late Cretaceous. However, their evolution during the Cretaceous remains poorly documented. Recent discoveries from the Hauterivian-Aptian interval suggest that the radiation of brachaucheniine pliosaurids produced a wide disparity of forms following the *Pliosaurus*-dominated assemblages of the Late Jurassic. Among the most bizarre of these early brachaucheniines is *Luskhan itilensis*, from the Hauterivian of Russia. We thoroughly describe the osteology of this tusked, longirostrine pliosaurid and discuss its possible behaviour by drawing comparisons with other marine amniotes possessing forward-pointing teeth. We use this opportunity to make extensive anatomical comparisons among Cretaceous pliosaurids, including previously overlooked cranial features. Bayesian inference of phylogenetic relationships of plesiosaurians reveals that the internal branches within Late Jurassic-Late Cretaceous pliosaurids have generally low rates of morphological evolution, indicating that the recently described Early Cretaceous pliosaurids have effectively bisected the long branch leading to the 'classical' brachaucheniines of the middle Cretaceous (*Kronosaurus*, *Brachauchenius*, *Megacephalosaurus*). Pliosaurids record very low evolutionary rates and a dwindling disparity prior to their extinction, mirroring the events seen – roughly at the same time – for ichthyosaurians.

INTRODUCTION

Pliosauridae is a long-lived clade of sauropterygian marine reptiles that have their first appearances in the fossil record during the Early Jurassic (Storrs & Taylor, 1996; Benson *et al.*, 2011a) or perhaps latest Triassic (Wintrich *et al.*, 2017). Early pliosaurids retained the plesiomorphic phenotype of plesiosaurians, with a small body size and an elongated neck (Benson, Evans, & Druckenmiller, 2012; Fischer *et al.*, 2020). Pliosaurids then evolved a large body size and a suite of predatory adaptations during the Middle Jurassic, with the appearance of the clade Thalassophonea (Ketchum & Benson, 2011a; Benson & Druckenmiller, 2014; Fischer *et al.*, 2020). Many thalassophoneans show craniodental traits associated with macropredators, suggesting that they mostly occupied the niche of apex predators of their respective food chains (e.g. Massare, 1987; McHenry, 2009; Fischer *et al.*, 2015, 2020). However, the recent discos of *Luskhan itilensis* from the late Hauterivian (Early Cretaceous) of Russia demonstrated the unexpected iterative evolution of a longirostrine phenotype among pliosaurids, revealing a wider disparity and colonisation of multiple trophic roles by the clade (Fischer *et al.*, 2017, 2020).

Despite their relevance to the structure of ancient marine ecosystems, our morphological understanding of pliosaurids is limited, because only a few taxa are represented by complete skeletons (Tutin & Butler, 2017), especially outside of a few, well-sampled Lagerstätten of the Jurassic (Benson *et al.*, 2010). Recently, a series of new discoveries from Russia (Fischer *et al.*, 2015, 2017; Zverkov *et al.*, 2018; Zverkov & Pervushov, 2020) and South America (Páramo-Fonseca *et al.*, 2016; Páramo-

Fonseca, Benavides-Cabra, & Gutiérrez, 2018; Gómez-Pérez & Noè, 2017) have expanded knowledge of pliosaurid evolution in the Cretaceous, following after the *Pliosaurus*-dominated assemblages of the Late Jurassic. *Luskhan itilensis*, from the Early Cretaceous of Russia is a crucial taxon because it is known by a remarkably complete skeleton (Fig. 1) from a poorly sampled stage (the Hauterivian) and also because it documents the early stages of the evolution of the last clade of pliosaurids, Brachaucheniinae (Fischer *et al.*, 2017). In this paper, we thoroughly describe the cranial and postcranial anatomy of *Luskhan itilensis* and assess its phylogenetic position with maximum parsimony and Bayesian inference. We use the Bayesian inference results to discuss the morphological evolutionary rates of pliosaurids from their origin around the Triassic-Jurassic boundary to their extinction during the early Late Cretaceous.

METHODS

Institutional abbreviations. **CAMSM**: Museum of Earth Sciences, University of Cambridge, Cambridge, UK; **CCNHM**: Mace Brown Museum College of Charleston, Charleston, South Carolina, USA; **IRSNB**: Royal Belgian Institute of Natural Sciences, Brussels, Belgium; **MNHN**: Muséum National d'Histoire Naturelle, Paris, France; **PETM**: Peterborough Museum & Art Gallery, Peterborough, England, UK; **PIN**: Paleontological Institute of the Russian Academy of Sciences, Moscow, Russia; **QM**: Queensland Museum, Hendra, Queensland, Australia; **USNM**: United States National Museum of Natural History, Smithsonian Institution, Washington DC, USA; **YKM**: Ulyanovskii Oblastnoi Kraevedcheskii Musei I.A. Goncharova (Ulyanovsk Regional Museum of Local Lore named after I.A. Goncharov), Ulyanovsk, Ulyanovsk Region, Russia.

Material. The holotype of *Luskhan itilensis*, YKM 68344/1_262, a subcomplete, semi-articulated, and three-dimensionally preserved skeleton. During the preparation of the remains, several kilos of the matrix located in the belly region have been sampled and macerated. Only a series of cephalopods hooklets have been recovered, but we consider this evidence as too scant for the unambiguous presence of gut content in the specimen.

Taxonomy. In a recent paper, Noè & Gómez-Pérez (2022) regarded the type material of the long-known thalassophonean taxon *Kronosaurus queenslandicus* as undiagnostic. However, the current knowledge of this taxon is based on a series of specimens that have been referred to *Kronosaurus queenslandicus* for decades (White, 1935; Romer & Lewis, 1959; Kear, 2003; McHenry, 2009). Instead of petitioning the ICZN to propose a neotype and maintain nomenclatural stability, Noè & Gómez-Pérez (2022) restricted the name *Kronosaurus queenslandicus* to the holotype specimen (QM F1609) and created a new genus and species, *Eiectus longmani*, for reception of the material housed in Harvard University (MCZ) and, "provisionally" (Noè & Gómez-Pérez, 2022: 6), for all other specimens assigned to *Kronosaurus* as well. We estimate that this course of action conflicts with the

recommendations in articles 75.5 and 75.6 of the ICZN and cannot be justified by the (otherwise sensible) possibility of multiple pliosaurid taxa in the Aptian-Albian deposits of Australia (Noè & Gómez-Pérez, 2022). As a result, we will use the name "*Kronosaurus-Eiectus*" for the material previously assigned to *Kronosaurus queenslandicus* in this contribution, pending further progress on this complex taxonomic issue.

3D scanning and modelling. We scanned the holotype of *Luskhan itilensis* using an handheld, high-definition structured light scanner (Artec Space Spider). We also scanned a series of important specimens of *Kronosaurus queenslandicus* (also referred to *Eiectus longmani* in Noè & Gómez-Pérez (2022)) from the QM, using a Creaform HandySCAN 300 laser surface scanner. All the 3D models are deposited in Morphosource: a 3D model of the symphysis of QM F10113 (0.8 mm resolution, www.morphosource.org/concern/media/000115328) and a 3D model a cast of the snout tip MCZ 1285 (0.2 mm resolution, www.morphosource.org/concern/media/000115329) have already been deposited by Fischer et al. (2020) (Morphosource project 0000C1018). We have also uploaded a 3D model of QM F2446 (0.5 mm resolution, www.morphosource.org/concern/media/000439494) and a 3D model of the "JCU" specimen (QM F51291) (0.2 mm resolution, www.morphosource.org/concern/media/000439605), as well as the holotype *Luskhan itilensis*, in several parts (0.25 mm resolution, link to the global project: http://www.morphosource.org/projects/000439440).

Phylogenetic analyses. We used the phylogenetic data matrix of Fischer et al. (2020) which is the most recent and most thorough dataset sampling pliosaurids. This matrix stems from Benson & Druckenmiller (2014) and has been updated in various subsequent works (Fischer *et al.*, 2015, 2017, 2018; Madzia, Sachs, & Lindgren, 2018; Páramo-Fonseca, Benavides-Cabra, & Gutiérrez, 2019). We analysed this dataset within a maximum parsimony and a Bayesian framework. Maximum parsimony analyses were carried on in TNT v1.5 (Goloboff & Catalano, 2016). In order to minimize the impact of homoplasy, we used the implied weighting method to change the weight of each character proportionally to their homoplasy. We used different values of the coefficient k (6, 9, and 12) to test for the influence of different strategies of character weighting: increasing the k value reduces the penalty applied to homoplastic characters. In a maximum parsimony framework, implied weighting appears a method of choice, providing accurate results (Goloboff *et al.*, 2018; Smith, 2019). We raised the maximum number of trees to 100,000 and used the New Technology Search (ratchet activated: 200 ratchet iterations; drift activated: 10 cycles; 5 hits; 10 trees per replication), to identify islands of most parsimonious trees. We applied the tree bisection-reconnection algorithm on the trees recovered by the ratchet analysis to fully explore these islands. We used a symmetric resampling of 33% change probability which gives the frequency differences for 10000 replicates to analyse the nodal support of our trees in an implied weighting framework. We used

the packages `ape` (Paradis *et al.*, 2004), `geoscale` (Bell & Lloyd, 2015), `paleotree` (Bapst, 2012), and `strap` (Bell & Lloyd, 2015) in the R v.4.0.3 statistical environment (R Core Team, 2016) to timescale the consensus tree a posteriori using the minimum branch length (mbl = 3) method and matrix of taxon ages (or, rather, the lower and upper boundaries of the uncertainty window surrounding the first record of each OTU), from Fischer et al. (2020). The matrix, the most parsimonious trees for each value of k, the R script, and the taxon age matrix are provided as supplementary files.

Bayesian inference of topology and clock rates were conducted jointly in MrBayes (v3.2.6) (Ronquist *et al.*, 2012). Character states were unweighted and unordered, and state frequencies were defined using a symmetrical Dirchlet hyperprior fixed at infinity which makes all state transitions equally likely. We set four runs of four chains, with a maximum of 200,000,000 generations, sampling at every 1000. We set a stop-value at 0.01, considering convergence is then reached. We applied a burn-in which discards the first 25% generations. We used the Mkv model with gamma rates and an uncorrelated relaxed clock (igr). We modified the clock rate based on the mean rate of character change per million year given by an analysis in maximum parsimony in equal weighting: a lognormal distribution with a mean of -1.82 and a variance of 0.5 and the prior on the variance of the independent gamma rate (igrvarpr) set at exp(1). We also used the fairly neutral fossilized birth death priors of Motani *et al*. (2017): fossilisation prior (fossilizationpr) as beta (1,150), sampling probability (sampleprob) as 0.1, specification prior (speciationpr) as exp(1), and extinction prior (extinctionpr) as beta (1,1). The full matrix with priors and inference protocol, the consensus tree (the .con.tre file), and all the outputs of the Bayesian Inference are provided as supplementary files.

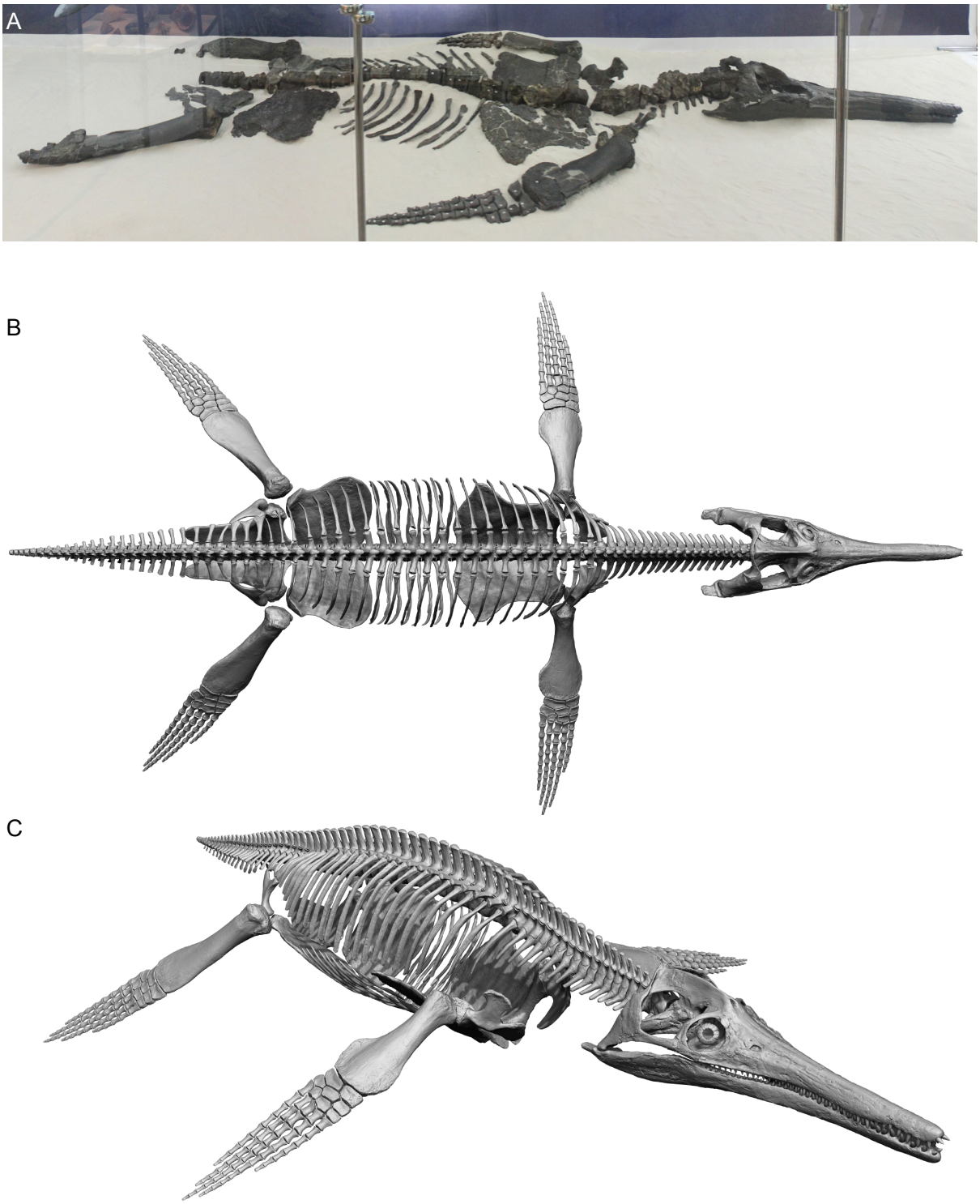

Figure 1. *Luskhan itilensis*, a remarkably complete pliosaurid from the Lower Cretaceous of Russia. A, display of the holotype (YKM 68344/1_262) in the YKM. B–C, 3D reconstruction of the skeleton of *Luskhan itilensis* in dorsal (B) and anterolateral (C) views. Please do not use this artistic reconstruction to describe anatomy or score phylogenetic characters.

Table 1. Cranial and appendicular measurements (in mm) from the holotype of *Luskhan itilensis* (YKM 68344/1_262).

	Length (anteroposterior)	**Height (dorsoventral)**	**Width (mediolateral)**
Mandible	1585	78*	
Symphysis	535		
Splenial, contribution to the symphysis	265		
Preorbital	940		130
Retroarticular	125		
Supratemporal fenestra	183		
Inter-quadrate distance	420		
Inter-retroarticular distance	435		
3rd dentary tooth basal diameter	22		
Neck length (with atlas-axis, without cartilage)	764		
Minimum trunk length (without cartilage)	1930		
Scapula	284		
Scapula, dorsal process		178	
Scapula, posterior (glenoid) process			147
Scapula, glenoid contribution	105		
Scapula-coracoid facet	73		
Coracoid	650	90**	615
Right forefin			1495
Right humerus, distally	165		645
Right humerus, mid shaft	295		
Left humerus, distally	307		625
Left humerus, mid shaft	160		
Radius	100		69
Ulna			65
Intermedium	93		57
Ischium	615		330
Ilium		240	
Pubis	515		620
Left femur, distal	285***		802
Left femur, mid shaft	165		
Right femur, mid shaft	177		805
Tibia	102		81
Fibula	137		87
Astragalus	90		58
Proximal phalange	52		69

*: taken at mid-snout; **: maximum height of the intercoracoid facet; ***: minimum value.

Table 2. Axial skeleton measurements (in mm) of the holotype of *Luskhan itilensis* (YKM 68344/1_262).

	Length (anteroposterior)	**Height (dorsoventral)**	**Width (mediolateral)**	**Height/Width**	**Height/Length**
Atlas	55	103	108	0.95	1.87
Atlantal intercentrum	55	NA	NA	NA	NA
Axis	43	95	107	0.89	2.21
Axial intercentrum	37	NA	NA		NA
Cervical 3	47	117	107	1.09	2.49
Cervical 4	42	100	103	0.97	2.38
Cervical 5	43	86	100	0.86	2.00
Cervical 6	46	92	102	0.90	2.00
Cervical 7	45	90	112	0.80	2.00
Cervical 8	46	90	111	0.81	1.96
Cervical 9	51	93	117	0.79	1.82
Cervical 10	52	93	115	0.81	1.79
Cervical 11	48	90	118	0.76	1.88
Cervical 12	47	93	113	0.82	1.98
Cervical 13	48	93	115	0.81	1.94
Cervical 14	50	95	107	0.89	1.90
Cervical 15	47	90	110	0.82	1.91
Pectoral1	54	97	115	0.84	1.80
Pectoral 2	56	95	117	0.81	1.70
Pectoral 3	55	93	114	0.82	1.69
Dorsal 1	61	90	113	0.80	1.48
Dorsal 2	67	92	103	0.89	1.37
Dorsal 3	70	98	102	0.96	1.40
Dorsal 4	74	93	110	0.85	1.26
Dorsal 5	85	101	105	0.96	1.19
Dorsal 6	90	106	112	0.95	1.18
Dorsal 7	86	105	110	0.95	1.22
Dorsal 8	80	95	92	1.03	1.19
Dorsal 9	78	100	98	1.02	1.28
Dorsal 10	78	100	112	0.89	1.28
Dorsal 11	80	100	115	0.87	1.25
Dorsal 12	82	102	110	0.93	1.24
Dorsal 13	83	103	114	0.90	1.24
Dorsal 14	87	102	100	1.02	1.17
Dorsal 15	80	103	107	0.96	1.29
Dorsal 16	81	100	108	0.93	1.23
Dorsal 17	84	100	107	0.93	1.19
Dorsal 18	80	100	106	0.94	1.25

Dorsal 19	81	100	107	0.93	1.23
Dorsal 20	NA	104	115	0.90	NA
Dorsal 21/Sacral1	75	90	NA		1.20
Dorsal 22/Sacral 2	80	93	100	0.93	1.16
Dorsal 23/Sacral 3	80	92	100	0.92	1.15
Dorsal 24/Sacral 4	77	92	115	0.80	1.19
Caudal 1	82	95	115	0.83	1.16
Caudal 2	75	95	112	0.85	1.27
Caudal 3	74	87	115	0.76	1.18
Caudal 4	70	85	110	0.77	1.21
Caudal 5	53	NA	NA	NA	NA

COMPARATIVE DESCRIPTION

Plesiosauria de Blainville, 1835
Pliosauridae Seeley, 1874
Thalassophonea Benson & Druckenmiller, 2014
Brachaucheniinae Williston, 1925 [sensu Benson & Druckenmiller, 2014]
Luskhan itilensis Fischer, Benson, Zverkov, Soul, Arkhangelsky, Lambert, Stenshin, Uspensky, Druckenmiller 2017

Figures 1–3, 5–12

Holotype. YKM 68344/1_262, a subcomplete, semi-articulated, and three-dimensionally preserved skeleton.

Locus typicus and stratum typicum. Upper portion of the *Speetoniceras versicolor* Zone, upper Hauterivian, Lower Cretaceous on the right bank of the Volga river, 3 km north of the Slantsevy Rudnik village, western Russia (Fischer *et al.*, 2017).

Note on diagnosis. The diagnosis of *Luskhan itilensis* remains unchanged compared to that of Fischer et al. (2017), with the exception that the number of premaxillary teeth is ambiguous, being either six or seven.

Rostrum. The holotype of *Luskhan itilensis* has longirostrine cranial proportions (Fischer *et al.*, 2017, 2020), with a preorbital rostrum accounting for 59% of the total skull length and a narrow snout (preorbital width/snout length = 0.2), comparable to the proportions of other longirostrine pliosaurids such as *Hauffiosaurus longirostris* (White, 1940; Benson *et al.*, 2011b; Fischer *et al.*, 2020), *Peloneustes* (Ketchum & Benson, 2011b), as well as some polycotylid plesiosaurians such as *Pahasapasaurus haasi* (Schumacher, 2007; Fischer *et al.*, 2017, 2020) and *Polycotylus latipinnis* (Schumacher & Martin, 2015) (see tables 1 – 2 for measurements). The rostrum is straight in dorsal view and lacks any mediolateral constriction at the anterior end of the premaxilla/maxilla contact. This is similar to the condition in some longirostrine pliosaurids such as *Marmornectes* (Ketchum & Benson, 2011a), and *Megacephalosaurus eulerti* (Schumacher, Carpenter, & Everhart, 2013). By contrast, a prominent constriction is seen in most Middle-Late Jurassic pliosaurids (Andrews, 1913; Tarlo, 1960; Ketchum & Benson, 2022) and, to a smaller extent, in *Kronosaurus–Eiectus* (McHenry, 2009). However, *Luskhan itilensis* exhibits a minute ventral expansion of the anterior portion of the maxilla, a feature again much more expressed in several latirostrine pliosaurids from the Late Jurassic (e.g. Andrews, 1913; Halstead, 1971; Brown, 1981; Noè, Smith, & Walton, 2004; Benson *et al.*, 2013) (it is also possibly present in *Marmornectes* (Ketchum & Benson, 2011a) and *Megacephalosaurus eulerti* (Schumacher *et al.*, 2013)). The dentary is dorsally convex anterior to this region.

Premaxilla. The premaxilla is elongated and slender, tapering anteriorly when seen in dorsal view, without any mediolateral expansion (Figs. 2, 3). The premaxilla is slightly dorsoventrally thicker at the level of its second alveoli than at the anterior emergence of the maxilla. Poor preservation of dental alveoli results in an uncertainty regarding the number of premaxillary teeth, which is either six or seven. Most premaxillary teeth are widely separated with interalveolar spaces that are longer anteroposteriorly than the alveolar lengths. Among thalassophoneans, widely spaced medial alveoli are also found in *Pliosaurus westburyensis* (R.B.J.B., pers. obs. of BRSMG Cc 332). The anteriormost premaxillary alveoli of *Luskhan itilensis* are small compared to more posterior alveoli. Nevertheless, they are less reduced than those of *Pliosaurus* and *Acostasaurus pavachoquensis*, in which the anteriormost alveolus is half the diameter of the third alveolus, or smaller (Benson *et al.*, 2013; Gómez-Pérez & Noè, 2017). As in *Makhaira rossica*, the anteriormost alveolus is not oriented ventrally but anteroventrally (Fischer *et al.*, 2015). However, this condition is much more strongly developed in *Luskhan itilensis*, resulting in a nearly horizontal, anteriorly projecting first premaxillary tooth. The interalveolar bone between the 1st and the 2nd alveolus is strongly thickened ventrally, creating a sort of bulbous buttress posterior to the 1st alveolus. A short, rectangular anteromedian trough is present between the anteriormost alveolus and the thickened interalveolar bone.

The anterolateral portion of the premaxilla-maxilla suture appears slightly crenulated. A crenulated morphology is also present in *Stenorhynchosaurus munozi* (Páramo-Fonseca *et al.*, 2016, 2019), *Sachicasaurus vitae* (Páramo-Fonseca *et al.*, 2018), and *Liopleurodon ferox* (R.B.J.B., pers. obs. of NHMUK R 2680) but this seemingly differs from the more pronounced zig-zag morphology seen in *Pliosaurus* spp. (Benson *et al.*, 2013), *Simolestes vorax* (R.B.J.B., pers. obs. PETMG R.296), and possibly *Acostasaurus pavachoquensis* (Gómez-Pérez & Noè, 2017). The suture extends linearly posteromedially from the alveolar margin of the jaw, forming the lateral margin of the posteromedian ('facial') process of the premaxilla. The premaxillae appear to be fused medially, lacking a clear inter-premaxillary suture. This condition is similar to that of *Stenorhynchosaurus munozi* (Páramo-Fonseca *et al.*, 2019) and is not observed in younger Cretaceous taxa (in which premaxillae are clearly separated by a straight suture throughout (Williston, 1907; McHenry, 2009; Schumacher *et al.*, 2013)). The premaxillae articulate with the parietals via a strongly interdigitating suture that is located directly medially to the external naris. This suture should not be confused with the numerous longitudinal ridges and furrows located further posteriorly, which texture the dorsal surface of the skull roof anterior to the parietal foramen. The anterior location of the premaxilla/parietal contact of *Luskhan itilensis* is a brachaucheniine synapomorphy (Benson & Druckenmiller, 2014) (which is however absent in *Acostasaurus pavachoquensis*; Gómez-Pérez & Noè, 2017), and differs from the condition of most other pliosaurids, in which the contact is located at the level of the anterior margin of the orbit (Andrews, 1913; Ketchum & Benson, 2011a; Benson *et al.*, 2013) or more posteriorly (Taylor & Cruickshank, 1993).

Maxilla. The anterior part of the maxilla is slightly expanded ventrolaterally (Figs. 2, 3), similar to that of *Megacephalosaurus eulerti* (Schumacher *et al.*, 2013). A more prominent ventral expansion of the maxilla is found in many Middle–Late Jurassic pliosaurids (Andrews, 1913; Benson *et al.*, 2013), notably in *Simolestes vorax* (R.B.J.B., pers. obs. on PETMG R.296; Noè, 2001). In *Acostasaurus pavachoquensis* the maxillary expansion is only lateral (Gómez-Pérez & Noè, 2017); *Stenorhynchosaurus munozi* seems to lack any marked maxillary expansion (Páramo-Fonseca *et al.*, 2016, 2019). Long longitudinal ridges and furrows texture the lateral surface of the maxilla at its mid-length. The contribution of the maxilla to the external naris cannot be assessed as the skull has been dorsoventrally crushed in that region. The maxilla forms a long, transversely compressed posteroventral process, which bears alveoli, and underlaps the 'lacrimal', and the anterior part of the jugal. This process extends posteriorly as far as the posterior margin of the orbit, as in *Pliosaurus kevani* (Benson *et al.*, 2013) and possibly *Stenorhynchosaurus munozi* (Páramo-Fonseca *et al.*, 2016). A series of narrow yet deep depressions are located along the ventral maxilla-'lacrimal' suture; but these appear distinct from the longer horizontal series of large foramina texturing the lateral surface of the posterior half of the maxilla seen in *Stenorhynchosaurus munozi* (Páramo-Fonseca *et al.*, 2019) and *Kronosaurus–Eiectus* (V.F., pers. obs. on QM F2446 an QM F51291).

Frontal. The frontals are, in places, difficult to discern due to imperfect preservation. However, their posteromedial contact with the parietal is obvious, forming an elongated surface with a rugose texture. Although this surface is present and similar on both sides of the skull, the full external exposure of the frontal cannot be assessed unambiguously (Figs 2, 3). The external exposure of the frontal seems to extend anteriorly up to the premaxilla-parietal suture. This condition would be similar to *Megacephalosaurus eulerti*, *Sachicasaurus vitae*, and *Stenorhynchosaurus munozi* (Schumacher *et al.*, 2013; Páramo-Fonseca *et al.*, 2018, 2019) and distinct from that of *Brachauchenius lucasi* and *Acostasaurus pavachoquensis* because the premaxilla-parietal suture appears to be located more posteriorly in these taxa (Schumacher *et al.*, 2013; Gómez-Pérez & Noè, 2017). In *Megacephalosaurus eulerti*, the frontal prominently interdigitate in the premaxilla-parietal suture (Schumacher *et al.*, 2013; Schumacher, pers. comm. September 2022)). Furthermore, the frontal of *Luskhan itilensis* does not contribute to the orbital rim dorsally, unlike in *Acostasaurus pavachoquensis* (Gómez-Pérez & Noè, 2017).

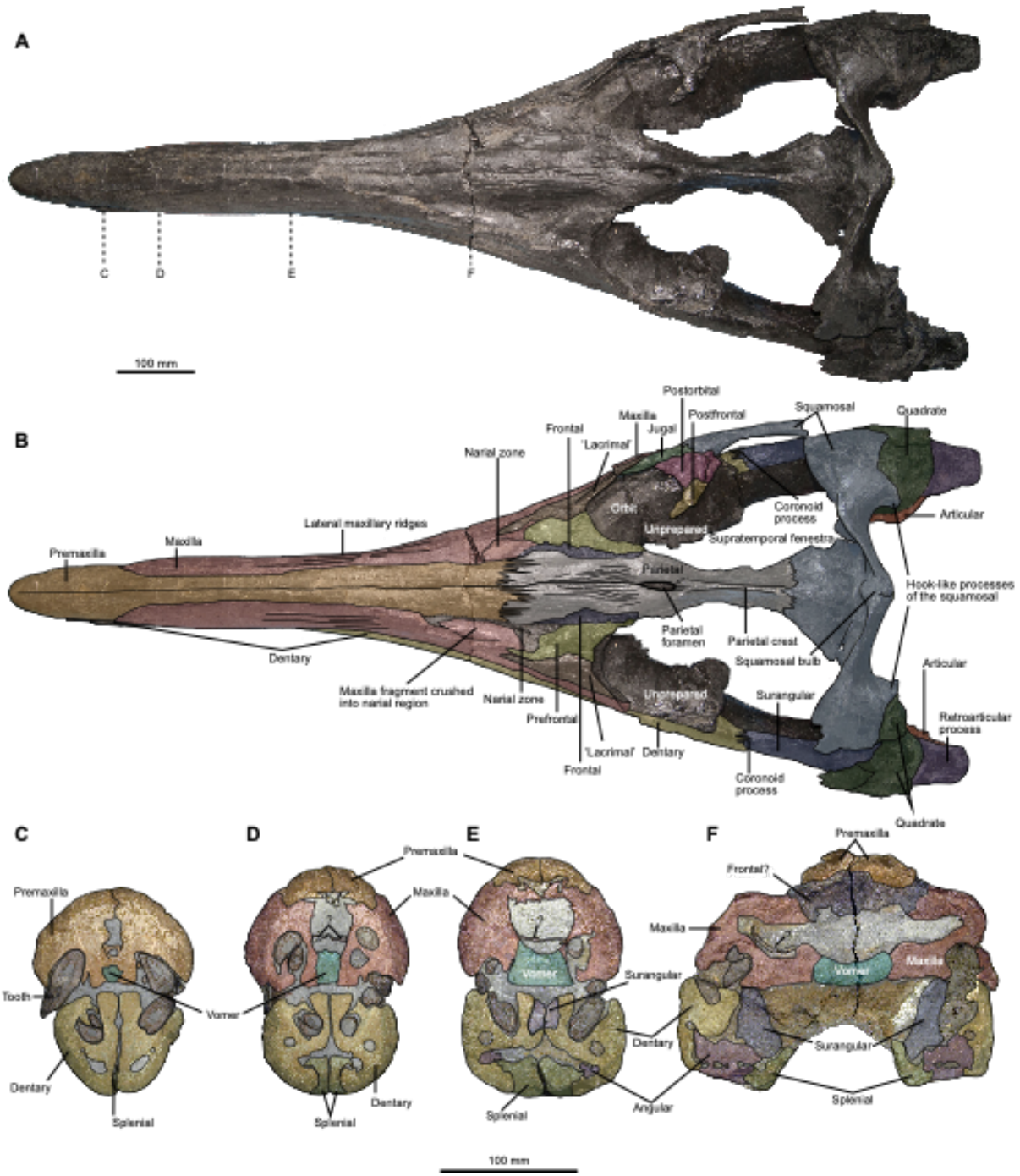

Figure 2. **Craniomandiobular osteology of the holotype of *Luskhan itilensis* (YKM 68344/1_262)**. A–B, photograph (A) and interpretation (B) of the skull in dorsal view. C–F, photograph and interpretation of four cross-sections (location indicated in (A). Uncertain sutures are indicated by a pitted line. The left postorbital bar and temporal arch are present but have not been photographed; it is present in Figure 3.

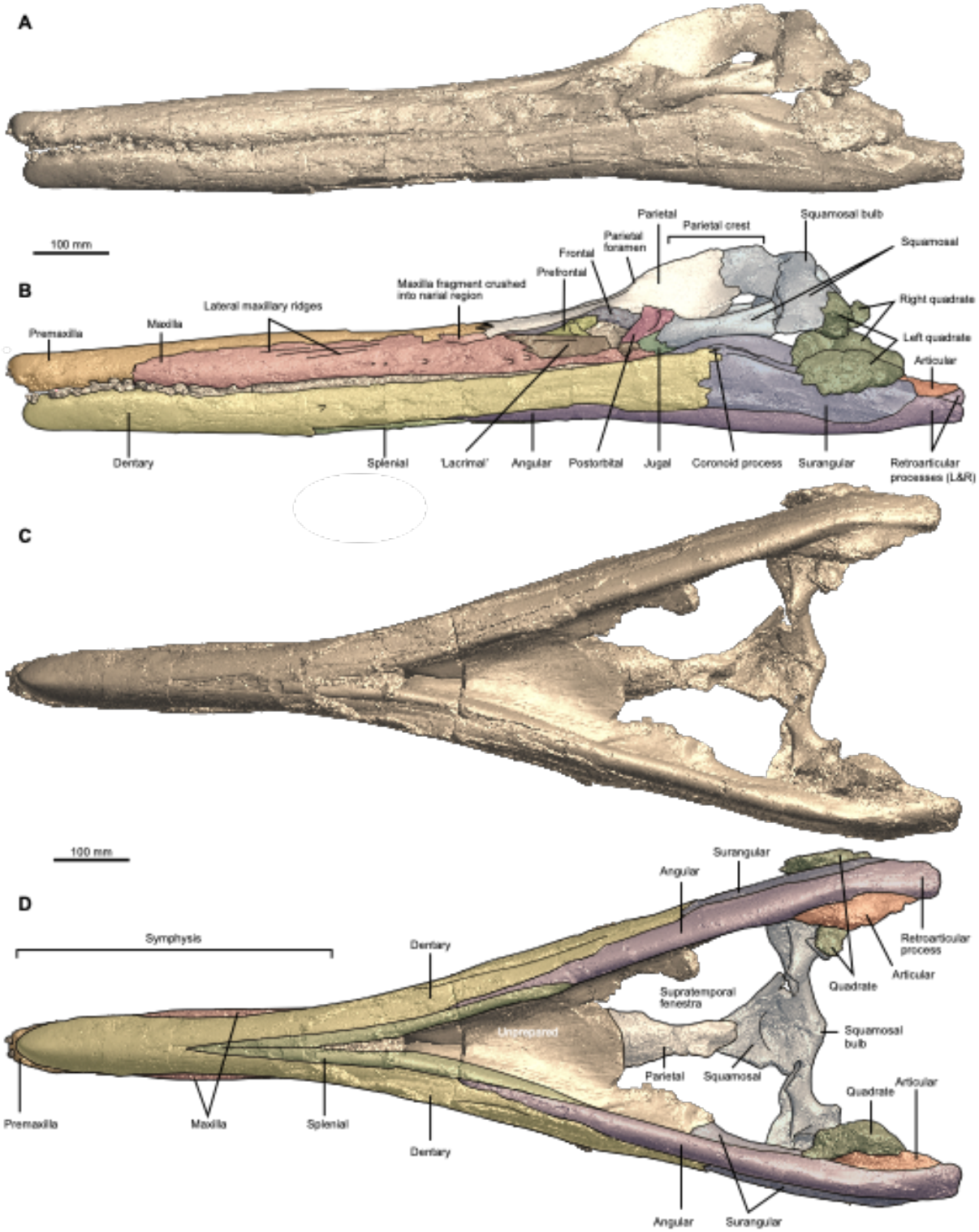

Figure 3. **Craniomandiobular osteology of the holotype of *Luskhan itilensis* (YKM 68344/1_262), based on a high-resolution 3D model**. A–B, photograph (A) and interpretation (B) of the skull in left lateral view. C–D, photograph (C) and interpretation (D) of the skull in ventral view. Uncertain sutures are indicated by a pitted line.

Orbital region. Pliosaurids exhibit a complex osteology in the anterior orbit-narial region, with the presence of numerous bones (Benson *et al.*, 2013), which have been assigned to the nasal, the 'lacrimal', the prefrontal, the palpebral, and neomorphic bones in the past (Williston, 1907; Ketchum & Benson, 2011b; Benson *et al.*, 2013). Different interpretations still co-exist among recent papers and remain to some extent unresolved, so the identities of these ossifications remain uncertain (Andrews, 1913; Ketchum & Benson, 2011b; Benson *et al.*, 2013; Schumacher *et al.*, 2013; Páramo-Fonseca *et al.*, 2019). We add to this discussion with observations of specimens referred to *Kronosaurus–Eiectus*, from the Early Cretaceous of Australia (QMF 2446, QMF 51291). These specimens clearly show the presence of at least two elements participating the anteroventral-to-anterodorsal orbit margin (Fig. 4). Element 1 forms the anteroventral orbit margin, including the anterior half of the ventral margin. It is delimited posteriorly by a crenulated suture with the jugal, at about mid-length of the ventral orbit margin. The existence of this suture has been debated (e.g. Carpenter, 1996; Ketchum & Benson, 2011b; Schumacher *et al.*, 2013), and it is possible that it varies among specimens. However, it is clearly visible on both left and right sides of QMF 51291, where this region is well-preserved (Fig. 4). Element 2 forms the entire anterior margin of the orbit. It contacts element 1 via a crenulated suture on both sides of both specimens QMF 2446 and QMF 51291. Most of the suture is situated inside the orbit; the lateral contact between these two elements is < 50 mm long (Fig. 4). Element 2 is extensive; it forms the posterior margin of the external narial aperture and extends dorsally and posteromedially, contacting, anteriorly to posteriorly the posterodorsal extremity of the maxilla, the frontal, and the postfrontal; the latter suture is crenulated distally. Element 2 is thick and pillar-like at the orbital margin. It is textured with numerous small circular foramina in between the orbit and the narial aperture, at least in the specimen QMF 51291 (Fig. 4). Just above the level of mid-orbit, element 2 forms a small dorsoventral ridge at the orbital margin; this process inserts into a furrow and is then separated from the dorsal part of the bone by a depression in specimen QMF 51291 (see pitted line in Fig. 4). In specimen QMF 2446, the dorsal part of element 2 is indistinguishable from the frontal. Yet, the small ridge dorsal to the pillar-like morphology is also visible in that specimen (Fig. 4). Accordingly, element 2 might constitute either one single element or two separate elements (see "prefrontal/'palpebral' in Fig. 4). However, aside from the pillar and furrow structure, the rest of the 'palpebral'-prefrontal suture – if present – is indiscernible in these specimens (QMF 2446, 51291), and it is possible that both these bones instead constitute a very large prefrontal, with varying bone textures. We use a 'two bones' colour scheme on our interpretation of *Kronosaurus–Eiectus* in Fig. 4 ('lacrimal' in brown, prefrontal in light green) and *Luskhan itilensis* (Figs 2, 3).

'Lacrimal'. The 'lacrimal' is a neomorphic bone (but see Noè, 2001) that excludes the maxilla from the anteroventral margin of the orbit, and has been identified by some authors in pliosaurids (Williston, 1907; Andrews, 1913; Benson *et al.*, 2011b, 2013; Ketchum & Benson, 2011b; Gómez-Pérez & Noè, 2017; Páramo-Fonseca *et al.*, 2019). Other authors regard this as a long anterior extension of the jugal (Taylor &

Cruickshank, 1993; Carpenter, 1996; O'Keefe, 2001; Schumacher *et al.*, 2013). This disagreement probably results from typically poor preservation of the suborbital bar in many pliosaurids, resulting difficulties in identifying the presence of a 'lacrimal'/jugal suture (see above in the specimen QMF 51291, *Kronosaurus–Eiectus*). In *Luskhan itilensis*, the jugal is clearly overlapped anterodorsally by a 'lacrimal' (Fig. 5). The 'lacrimal' is a low triangular bone with a long transversely compressed and dorsally tapering process contacting the posterior process of the maxilla (Figs 2, 3). The 'lacrimal' also forms a long, transversely compressed anterior process contacting the lateral surface of the maxilla, as in *Kronosaurus–Eiectus* (McHenry, 2009). This process appears much shorter in *Stenorhynchosaurus munozi* (Páramo-Fonseca *et al.*, 2019). The suture between the 'lacrimal' and prefrontal/palpebral is located ventral to mid-orbit height, as usually the case in thalassophoneans (Ketchum & Benson, 2011b; Benson *et al.*, 2013; Madzia *et al.*, 2018).

Prefrontal. The prefrontal is a large triangular bone with a long transversely compressed anteroventral process (Figs 2, 3). Due to poor preservation, it is difficult to determine whether the prefrontal extends to contact the posterior margin of the external naris, but it is likely the case given the length of the anterior process. *Brachauchenius lucasi*, *Megacephalosaurus eulerti* and *Stenorhynchosaurus munozi* also possess an anterior process of the prefrontal that contacts the external naris (Schumacher *et al.*, 2013; Páramo-Fonseca *et al.*, 2019). This contact is absent in some earlier thalassophoneans, including *Peloneustes* and *Pliosaurus*, because the frontal extends anteroventrally to contact the maxilla in these forms, excluding the prefrontal from the posterior margin of the external naris; this condition is supposedly the plesiomorphic one (e.g. Taylor & Cruickshank 1993; Ketchum & Benson 2011b; Benson *et al.*, 2013) The lateral surface of the prefrontal appears slightly concave in *Luskhan itlensis*. The prefrontal contacts the frontal dorsally and the right prefrontal seems to contact the parietal as well, although the absence of well-preserved postfrontals makes this interpretation ambiguous. In its posterodorsal region, the prefrontal forms a small convexity that projects into the dorsal orbit margin. This also occurs in various other thalassophoneans, in which a prominent convexity of the prefrontal projects into the anterodorsal or dorsal orbit margin (e.g. Andrews, 1913; Ketchum & Benson, 2011b; Gómez-Pérez & Noè, 2017 [where is it termed 'orbital flange']).

Jugal. The jugal is transversely compressed, with a dorsoventrally oval cross-section and a very limited lateral exposure; the medial exposure is larger (Figs. 2, 3, 5). The anterior portion of the jugal is anterolaterally overlapped by the sheet-like posterior processes of the 'lacrimal'. This condition differs from *Pliosaurus kevani*, *Megacephalosaurus eulerti*, and *Kronosaurus–Eiectus*, where the 'lacrimal' does not overlap the jugal extensively (Benson *et al.*, 2013; Madzia *et al.*, 2018; this work). The jugal/squamosal suture is crenulated, and the jugal projects a small and flat medioventral posterior process underlapping the anterior part of the squamosal (Fig. 5). This condition appears quite similar to that of *Pliosaurus kevani*, although the

posterior process of the jugal of *Luskhan itilensis* is located medioventrally rather than strictly ventrally in *Pliosaurus kevani* (Benson *et al.*, 2013).

Postfrontal. Only a posteroventral fragment of the right postfrontal is preserved, forming the dorsal portion of the postorbital bar and contacting the postorbital ventrally in a ventrally-convex suture (Fig. 5). The cross-section of lateral process, which contacts the postorbital, is thick and pillar-like.

Postorbital. The postorbital is mediolaterally thin and has a concave anterior margin that forms the posteroventral portion of the posterior orbit margin, and a straight, posterodorsally-facing posterior surface that forms part of the margin of the temporal fenestra (Fig. 5). The ventral surface of the postorbital contacts the jugal anteriorly and the squamosal posteriorly, so the jugal is excluded from participation in the margin of the temporal fenestra. This condition is present in most plesiosaurians, but is unlike the condition in the Late Cretaceous pliosaurids *Megacephalosaurus eulerti* and *Brachauchenius lucasi*, in which a postorbital/squamosal contact is absent (McHenry, 2009; Schumacher *et al.*, 2013). The lateral surface of the postorbital is smooth and slightly concave and the posterior part of the postorbital is strongly thickened, with a squared cross-section. The medial surface of the postorbital is rugose.

Parietal. The anterior process of the parietal extends far anteriorly, reaching the level of the external naris (Fig. 2), as in *Brachauchenius lucasi* and *Megacephalosaurus eulerti* (Williston, 1907; Schumacher *et al.*, 2013) and thus slightly more anteriorly than in *Kronosaurus–Eiectus* and *Stenorhynchosaurus munozi* (McHenry, 2009; Páramo-Fonseca *et al.*, 2019), and much more anteriorly than in *Acostasaurus pavachoquensis* (Gómez-Pérez & Noè, 2017). The dorsal surface of the parietal anterior to the parietal foramen is textured by deep ridges and furrows, as are commonly present in thalassophoneans (e.g. Ketchum & Benson, 2011b). Some ridges converge posteromedially near the parietal foramen, while the anterior ridges, at the level of the premaxilla-parietal suture are longitudinal. A large parietal foramen is present; its dorsal edge is also textured by fine ridges; its position is slightly anterior to the level of the postorbital bar; these two structures are aligned in *Kronosaurus–Eiectus*, *Pliosaurus patagonicus* and *Stenorhynchosaurus munozi* (McHenry, 2009; Gasparini & O'Gorman, 2014; Páramo-Fonseca *et al.*, 2019). The parietal crest is tall along its entire length (113mm), extending dorsal to the more anterior portions of the skull roof as a sharp ridge. Its dorsal margin is straight and oriented anteroventrally. The parietal crest reaches the squamosal arch posteriorly, as in *Pliosaurus kevani* and unlike in *Acostasaurus pavachoquensis* where it is short and convex (Benson *et al.*, 2013; Gómez-Pérez & Noè, 2017). The parietal crest is also short and convex in *Megacephalosaurus eulerti*, but it does rearch the squamosal (Schumacher *et al.*, 2013). The ventral surface of the parietal vault is partly broken, but a deep concave posterior portion receiving the brain and the supraoccipital is present. The parietal-squamosal suture is obliterated by bony fusion.

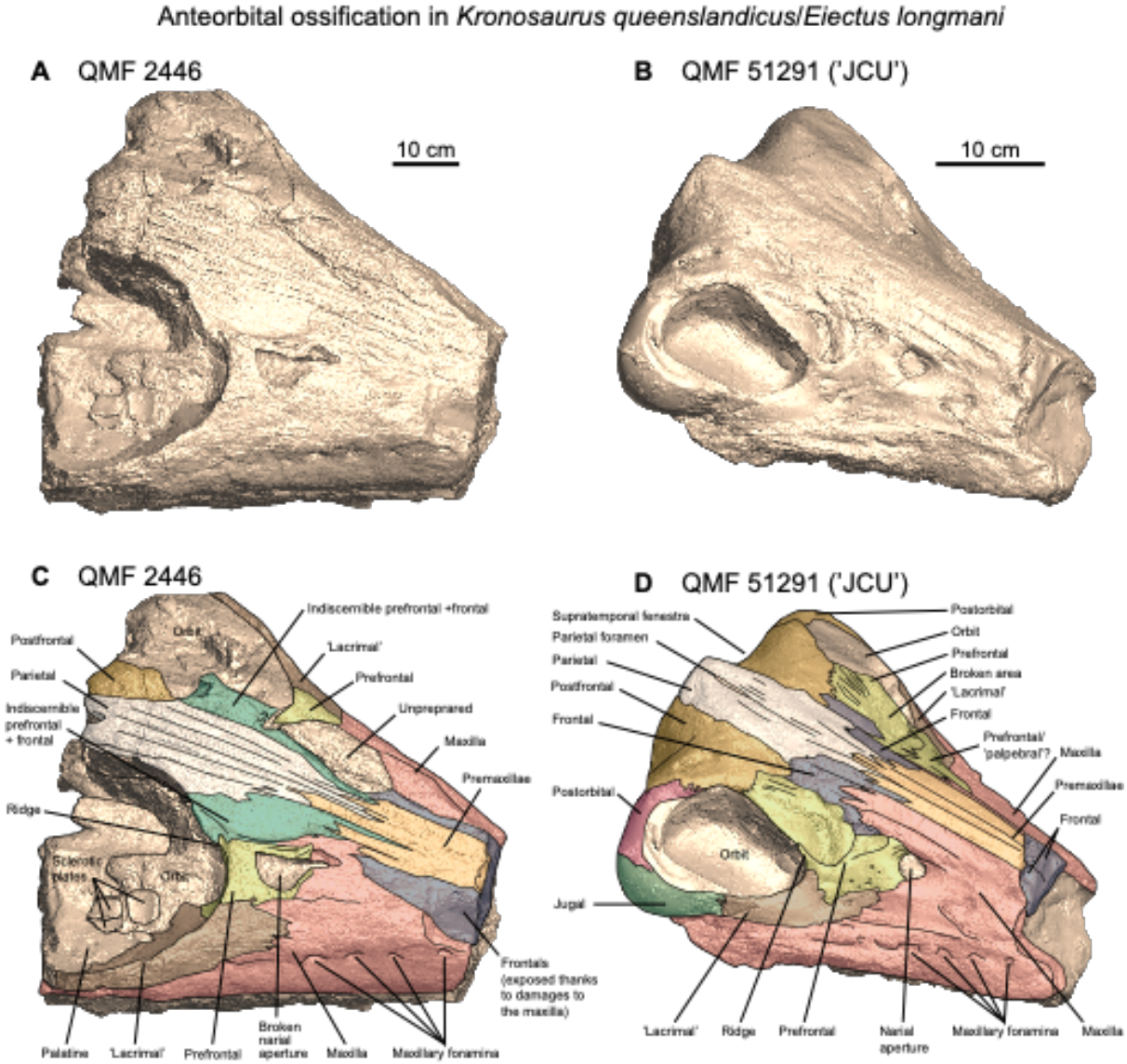

Figure. 4. **Cranial osteology of *Kronosaurus–Eiectus* based on high-resolution 3D models**. A–C, photograph (A) and interpretation (C) of QMF 2446 in dorsolateral view. B–D, photograph (B) and interpretation (D) of QMF 51291 in dorsolateral view. Uncertain sutures are indicated by a pitted line.

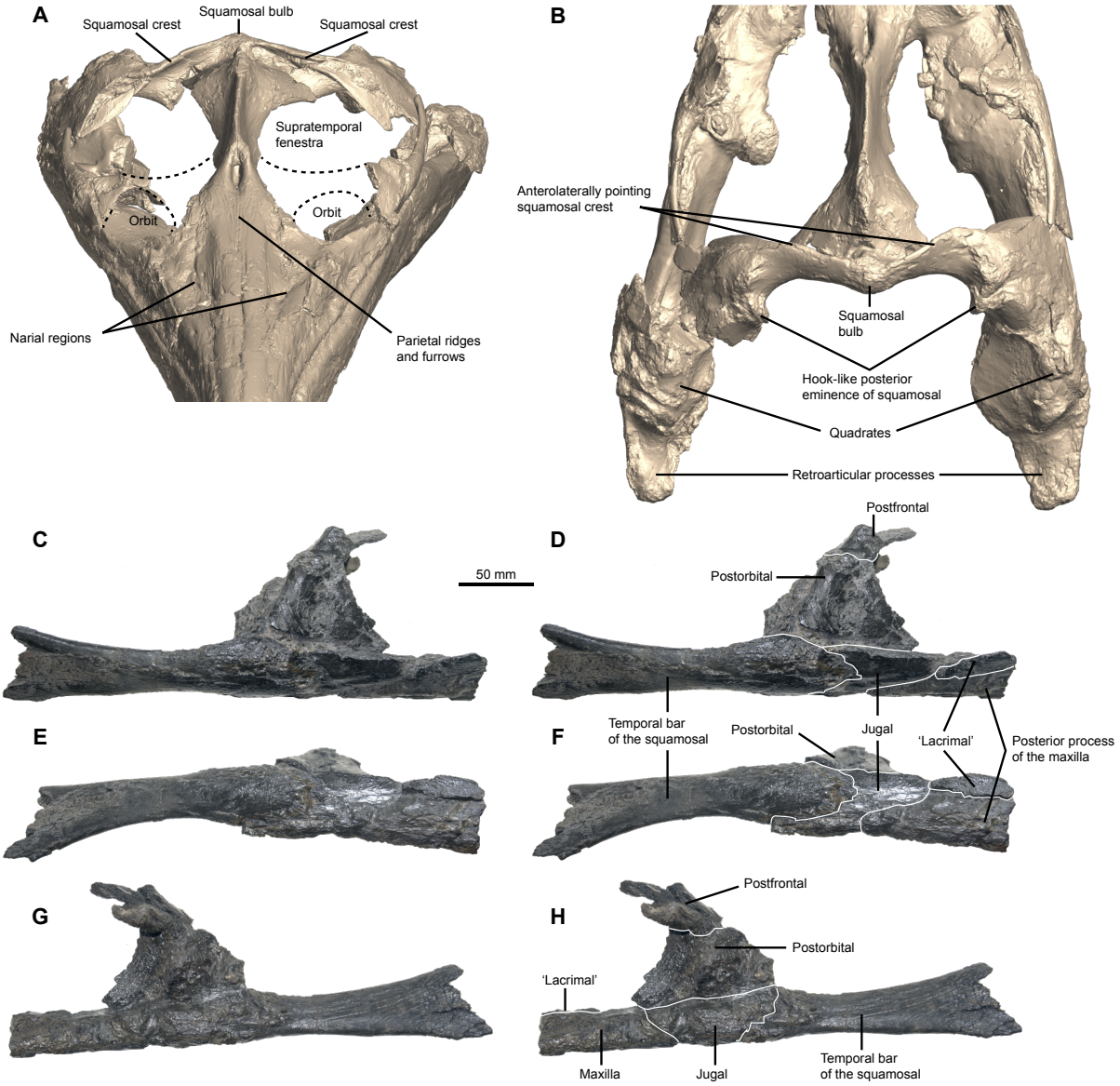

Figure 5. Orbital and postorbital regions of the holotype of *Luskhan itilensis* (YKM 68344/1_262). A, orbital and postorbital regions of a high-resolution 3D model, in anterodorsal view. The extent of the orbit and supratemporal fenestra is reconstructed by the pitted line. B, Postorbital region in dorsal view. C–H, photographs and interpretations of the right postorbital and temporal bars in lateral (C, D), ventral (E, F), and medial (G, H) views.

Squamosal. The dorsal processes of the squamosals contact medially posterior to the parietals. The squamosals extend anteriorly and posteriorly at this contact, forming a prominent and rugose 'squamosal bulb' (Figs. 2, 5), a widespread feature among early plesiosaurians and pliosaurids (O'Keefe, 2001: character 55). However, it is especially prominent in *Luskhan itilensis* (e.g. more so than in *Pliosaurus patagonicus*, *Megacephalosaurus eulerti*, and *Acostasaurus pavachoquensis* (Schumacher *et al.*, 2013; Gasparini & O'Gorman, 2014; Gómez-Pérez & Noè, 2017)). This process seems to disappear in some derived brachaucheniines (*Brachauchenius lucasi*, and possibly *Kronosaurus–Eiectus* (McHenry, 2009)). Similarly, *Luskhan itilensis* retains a mediolaterally oriented squamosal crest as in Jurassic thalassophoneans and unlike in *Acostasaurus pavachoquensis* (Gómez-Pérez & Noè, 2017) and more derived brachaucheniines ((Benson & Druckenmiller, 2014): character 54). The posterior surface of each dorsal process is concave, giving the squamosal arch a marked bow shape in dorsal view. The medial half of the squamosal crest even points anterolaterally in *Luskhan itilensis*; this orientation and shape is similar to polycotylids such as *Dolichorhynchops* (Sato, 2005; Sato *et al.*, 2011), but differs from other pliosaurids, in which the squamosals extend laterally or posterolaterally from their median contact (Andrews, 1913; Benson *et al.*, 2013; Schumacher *et al.*, 2013; Gómez-Pérez & Noè, 2017). The posterior surface of the squamosal extends posteroventrally at the squamosal-quadrate suture to form a recurved, hook-like process bearing a broad, rugose posterolateral bulge (Figs. 2, 5). This is likely homologous with the rugose eminences seen on the posterior surface of the squamosal in some other pliosaurids, including *Hauffiosaurus* spp. (Benson *et al.*, 2011b) and many species of *Pliosaurus* (Benson *et al.*, 2013). Such a rugose eminence appears absent in *Pliosaurus patagonicus* (Gasparini & O'Gorman, 2014). Laterally, the squamosal is mediolaterally thin and sheet-like, forming the ventral process that covers the lateral surface of the quadrate, and anterior process, which forms the temporal bar, and contacts the jugal and the postorbital anteriorly. This squamosal-postorbital contact excludes the jugal from the temporal fenestra, unlike in *Brachauchenius lucasi* and *Megacephalosaurus eulerti* (Albright, Gillette, & Titus, 2007; Schumacher *et al.*, 2013). The temporal bar is straight, transversely compressed and expands posteriorly. Its lateral surface becomes slightly concave posterior to mid length of the temporal fenestra. The posterior portion of squamosal/parietal vault is mediolaterally broad, equal to approximately half the width of the cranium as in *Pliosaurus* spp. (Benson *et al.*, 2013).

Quadrate. Both quadrates are complete but fractured (Figs. 2, 3, 5). The dorsal part of the quadrate is rectangular in cross-section, with a mediolateral long axis. The ventral (articular) end is expanded posteriorly, medially and anteriorly, and possesses a squared cross-section with a concave posterior surface. A shallow groove borders the posterodorsal margin of the glenoid surface. The squamosal and quadrate appear partly fused, making it difficult to determine the exact location of the squamosal-quadrate suture.

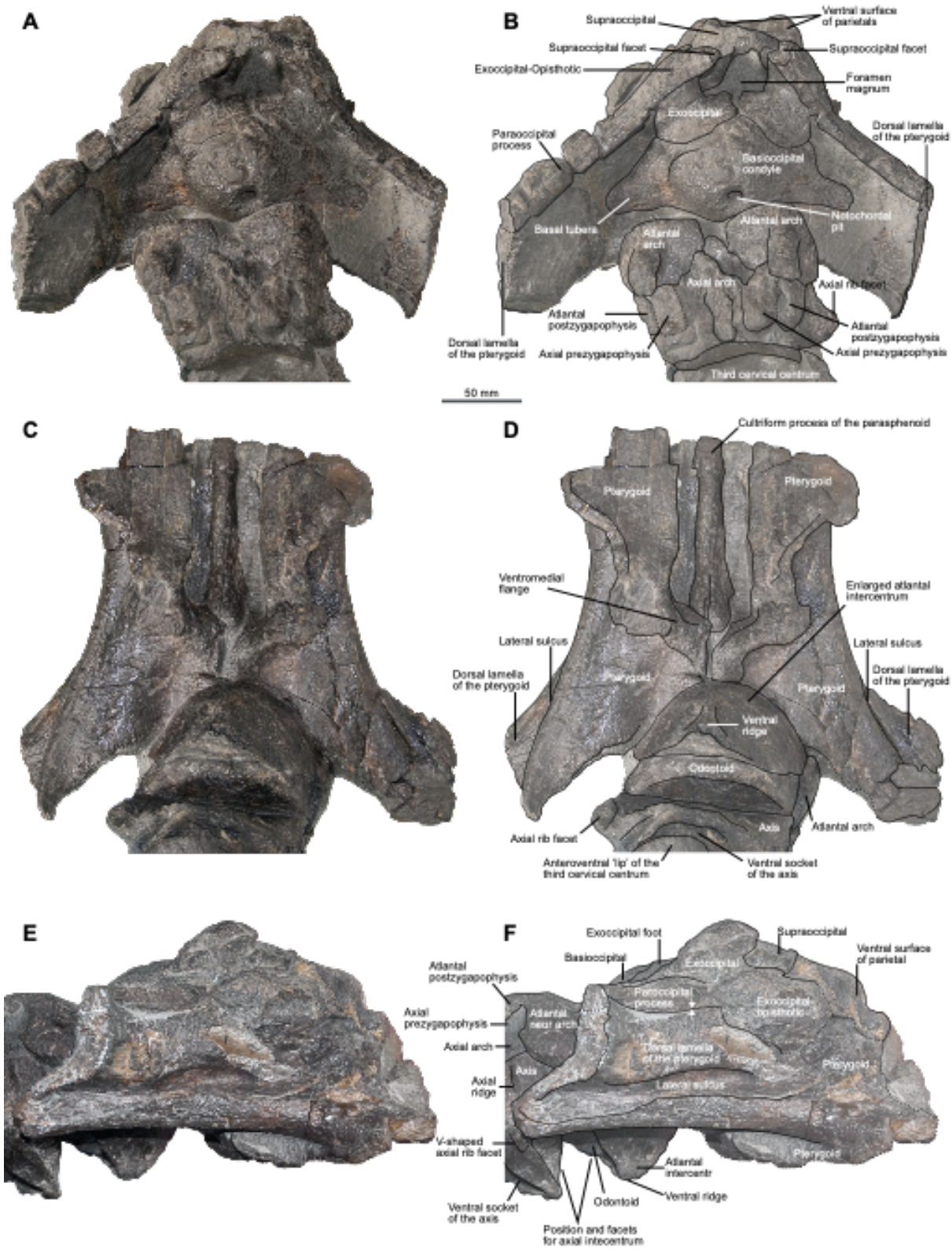

Figure 6. **Basicranium of the holotype of *Luskhan itilensis* (YKM 68344/1_262)**. Photographs and interpretations of the basicranium in posterodorsal (A, B), ventral (C, D), and left lateral (E, F) views.

Basioccipital. The basioccipital is only partly exposed; articulation with the atlas-axis complex covers its posteroventral portion (Fig. 6). The basioccipital condyle is rounded (81 mm in horizontal diameter), as in *Peloneustes philarchus* and *Acostasaurus pavachoquensis* (Ketchum & Benson, 2011b; Gómez-Pérez & Noè, 2017) and unlike in *Pliosaurus almanzaensis* and *Kronosaurus–Eiectus*, in which it is markedly oval (White, 1935; O'Gorman, Gasparini, & Spalletti, 2018). The basioccipital bears a large notochordal pit, unlike in *Pliosaurus* and *Kronosaurus–Eiectus*, which lack such a feature (White, 1935; Benson *et al.*, 2013; O'Gorman *et al.*, 2018). The extracondylar area, comprising the basal tubera, merges continuously with the occipital condyle; a condylar peripheral groove is absent at least dorsally and laterally – the ventral region cannot be observed. The basal tubera expand laterally below the level of the notochordal pit/central point of the condyle as in *Pliosaurus almanzaensis* and *Kronosaurus–Eiectus* (White, 1935; O'Gorman *et al.*, 2018); this lateral expansion starts dorsal to the notochordal pit in *Peloneustes philarchus* (Ketchum & Benson, 2011b).

Exoccipital-opisthotic. The ventral 'feet' of the exoccipitals, which articulate ventrally with the basioccipital, are strongly expanded medially, contacting each other on the midline, and thereby excluding the basioccipital from the floor of the foramen magnum (Fig. 6). This is unlike the situation in other plesiosaurians, including pliosaurids such as *Peloneustes philarchus* (Andrews, 1913), *Liopleurodon ferox* (Andrews, 1913), *Pliosaurus almanzaensis* (O'Gorman *et al.*, 2018), *Acostasaurus pavachoquensis* (Gómez-Pérez & Noè, 2017) and likely *Kronosaurus–Eiectus* (White, 1935). The foramen for cranial nerve XII is present on the medial surface, but the presence of other exoccipital foramina cannot be assessed due to imperfect preservation and incomplete removal of the matrix. The exoccipital expands dorsomedially to form the supraoccipital facet. The cross-section of the paroccipital process is dorsoventrally compressed as in *Pliosaurus* (Benson *et al.*, 2013) and, presumably, *Acostasaurus pavachoquensis* (Gómez-Pérez & Noè, 2017), but unlike in *Peloneustes philarchus* (Ketchum & Benson, 2011b). The anterolateral edge of the paroccipital process is straight while its posteromedial edge is concave in dorsal view; its dorsal surface is also concave, when seen in posterior view. The ventral surface of the paraoccipital process is in close contact with the dorsal surface of the quadrate ramus of the pterygoid along its entire length. This is unlike the situation in most other plesiosaurians, including the pliosaurids *Peloneustes philarchus* (Ketchum & Benson, 2011b) and *Kronosaurus–Eiectus* (White, 1935), in which only the distal end of the paraoccipital process contacts the posterior surface of the pterygoid on the occipital surface of the skull. Such a continuous contact between the paraoccipital process and quadrate ramus of the pterygoid is only found in *Luskhan itilensis* and *Pliosaurus westburyensis* (R.B.J.B., pers. obs. on BRSMG Cc332).

Supraoccipital. The supraoccipital has been crushed and rotated anteroventrally, so that its originally vertical axis is now horizontal (Fig. 6). It lies on the dorsal surface of the basicranium and is covered anteriorly by a fragment of the ventral surface of the

parietal and by the dorsal extremity of the dorsal lamella of the posterior ramus of the pterygoid. Unlike in other thalassophoneans, including *Peloneustes philarchus* (Andrews, 1913; Ketchum & Benson, 2011b), *Kronosaurus–Eiectus* (White, 1935) and *Pliosaurus kevani* (Benson *et al.*, 2013), the ventral margin of the supraoccipital is strongly embayed by the foramen magnum, resulting in a teardrop-shaped foramen magnum. A strongly embayed ventral margin is also present in the supraoccipital of *Pliosaurus westburyensis* (R.B.J.B., pers. obs. on BRSMG Cc332).

Parabasisphenoid. The posterior portion of the basicranium is preserved, including most of the posterior interpterygoid vacuity. This cavity is divided on the midline by the parabasisphenoid, which is mediolaterally convex in that region (Fig. 6). A shallow keel is present ventrally (thus perhaps similar to *Pliosaurus almanzaensis*, which possesses a triangular cross-section of the parasphenoid; (O'Gorman *et al.*, 2018). The parasphenoid becomes transversely thicker posteriorly, where its ventral surface becomes rugose and textured by small ridges and furrows. The parasphenoid of *Luskhan itilensis* appears much more robust than that of *Stenorhynchosaurus munozi* (Páramo-Fonseca *et al.*, 2016, 2019). The rounded ventral surface of the parabasisphenoid is similar to the conditions seen in *Brachauchenius lucasi* (McHenry, 2009; Schumacher *et al.*, 2013)*, Megacephalosaurus eulerti* (Schumacher *et al.*, 2013), *Kronosaurus–Eiectus* (White, 1935), *Gallardosaurus iturradlei* (Gasparini, 2009), *Pliosaurus westburyensis* (Taylor & Cruickshank, 1993), and likely *Stenorhynchosaurus munozi* (Páramo-Fonseca *et al.*, 2016), but is unlike the sharp midline keels seen in Middle Jurassic thalassophoneans (Andrews, 1913; Ketchum & Benson, 2011b, 2022) and some species of *Pliosaurus* (Benson *et al.*, 2013). In the middle-Cretaceous brachaucheniines *Brachauchenius lucasi* (Williston, 1907; McHenry, 2009; Schumacher *et al.*, 2013)*, Megacephalosaurus eulerti* (Schumacher *et al.*, 2013), and *Kronosaurus–Eiectus* (White, 1935), the contact between the parabasisphenoid and basioccipital is visible posteriorly, on the ventral surface of the basicranium. However, in *Luskhan itilensis*, this contact is not visible, and is presumably covered by the pterygoids posteriorly to the posterior interpterygoid vacuity. This condition is similar to that seen in earlier thalassophoneans (Andrews, 1913; Taylor & Cruickshank, 1993; Ketchum & Benson, 2011b; Gómez-Pérez & Noè, 2017; O'Gorman *et al.*, 2018).

Pterygoid. The posterior parts of both pterygoids are preserved in anatomical connection and articulated with the basicranium (Fig. 6). The pterygoids contact each other on the midline posterior to the posterior interpterygoid vacuity, in a long median contact that obscures the entire ventral surface of the basioccipital and the posterior portion of the parabasisphenoid. The posterior interpterygoid vacuity is anteroposteriorly long (preserved portion = 106.6 mm) compared to its mediolateral width (50.8 mm), yielding a minimum length:width ratio of 2.1, which is high compared to that of *Liopleurodon ferox* (Andrews, 1913) but in the range to that of other pliosaurids, such as *Peloneustes philarchus* (Ketchum & Benson, 2011b), *Eardasaurus powelli* (Ketchum & Benson, 2022), *Pliosaurus alamanzaensis*

(O'Gorman *et al.*, 2018), *Stenorhynchosaurus munozi* (Páramo-Fonseca *et al.*, 2016, 2019), *Acostasaurus pavachoquensis* (Gómez-Pérez & Noè, 2017), *Sachicasaurus vitae* (Páramo-Fonseca *et al.*, 2018), and *Kronosaurus–Eiectus* (White, 1935). The preserved portion of the posterior interpterygoid vacuity clearly extends anteriorly past the anterior margin of the subtemporal fossa (i.e. the posterior margin of the main portion of the palate), indicating that the original mid-length of the posterior interpterygoid vacuity was located approximately level with – or anterior to – the anterior margin of the subtemporal fossa, as seen in thalassophoneans in the clade comprising *Simolestes vorax*, *Liopleurodon ferox*, *Gallardosaurus iturraldei*, *Pliosaurus* spp. and brachaucheniines (Williston, 1907; Andrews, 1913; White, 1935; Taylor & Cruickshank, 1993; Gasparini, 2009; Páramo-Fonseca *et al.*, 2016), as well as in leptocleidids (Smith & Dyke, 2008: character 43).

Laterally, and posteriorly to the posterior interpterygoid vacuity, the ventral surface of the pterygoid bears a broad, curved, and ventrolaterally oriented flange, which extends posteromedially from the base of the lateral process of the pterygoid (Fig. 6D). This flange is present in all thalassophoneans (Williston, 1907; Andrews, 1913; Ketchum & Benson, 2011b) and in *Microcleidus* (Brown, Vincent, & Bardet, 2013). In *Luskhan itilensis* and most other thalassophoneans (Ketchum & Benson, 2011b; Schumacher *et al.*, 2013; Páramo-Fonseca *et al.*, 2018), the flanges on each pterygoid contact each other on the midline posterior to the interpterygoid vacuity. This is unlike the condition in *Brachauchenius lucasi*, in which the flanges are separated across the midline by a wide gap (Williston, 1907).

The quadrate ramus of the pterygoid is L-shaped in cross-section, forming a high and transversely thick dorsal lamella covering the lateral and laterodorsal surfaces of the basicranium anterior to the exoccipital and buttressing the paroccipital process of the opisthotic posterolaterally (Fig. 6F). We find no evidence for a fossa between dorsal lamella of the pterygoid and the exoccipital-opisthotic, as in *Pliosaurus westburyensis* (R.B.J.B., pers. obs. of BRSMG Cc 332). A deep anteroposterior sulcus is present laterally, at the base of the dorsal lamella of the posterior pterygoid ramus.

Mandible. Pyrite has damaged the medial surface of the mandible anteriorly and the lateral part of the palate is crushed onto the dorsomedial surface of the mandible; it is thus impossible to describe the medial morphology of the mandible. The lateral surface of the mandible is not markedly bowed (Fig. 3), as in *Pliosaurus patagonicus* (Gasparini & O'Gorman, 2014) and *Pliosaurus almanzaensis* (O'Gorman *et al.*, 2018), and brachaucheniines in general (Williston, 1907; McHenry, 2009; Angst & Bardet, 2016; Holland, 2018; Páramo-Fonseca *et al.*, 2019; Noè & Gómez-Pérez, 2022), with the exception of *Acostasaurus pavachoquensis* (Gómez-Pérez & Noè, 2017). The relative symphysial length is proportionally longer than in any other pliosaurid, with a proportional length of 0.337 of the total mandible length (it is 0.3 in *Marmornectes candrewi* (Ketchum & Benson, 2011a), 0.28 in *Peloneustes philarchus* [GPIT03182; see (Fischer *et al.*, 2017, 2020)], 0.27 in *Pliosaurus brachyspondylus* [CAMSM J35991; (Tarlo, 1959a) and below 0.25 in all other pliosaurids (Fischer *et al.*, 2020)). The number of dentary alveoli encompassed by the symphysis is difficult to count

because of pyrite filling and the general fragility of the material but appears well above 10 and probably close to 15, which would be similar to *Marmornectes crandrewi*, *Peloneustes philarchus*, and *Pliosaurus kevani* (Ketchum & Benson, 2011a,b; Benson *et al.*, 2013). As in the premaxilla, the symphysial dentary teeth are however widely spaced, with interalveolar spaces that are greater in length than the alveolar diameters (Fig. 3). As a result, even with a estimation of 15 symphysial teeth, *Luskhan itilensis* would have a low density of symphysial teeth (0.28 tooth per cm); such a value is otherwise only found in taxa with a few very large teeth: *Pliosaurus carpenteri* (0.2) (Knutsen, 2012; Sassoon, Noè, & Benton, 2012; Fischer *et al.*, 2017), *Pliosaurus brachydeirus* (0.28) (Knutsen, 2012; Fischer *et al.*, 2017), *Pliosaurus brachyspondylus* (0.27) (Tarlo, 1959a, 1960; Knutsen, 2012; Fischer *et al.*, 2017), *Kronosaurus–Eiectus* (0.19) (McHenry, 2009; Fischer *et al.*, 2017, 2020; Holland, 2018), and *Megacephalosaurus eulerti* (0.21) (Fischer *et al.*, 2020).

Dentary. The dentary is elongated. Its anterior portion is not spatulated (Figs. 2, 3), unlike in many other thalassophoneans, but similar to the condition in *Marmornectes candrewi* (Ketchum & Benson, 2011a), *Brachauchenius lucasi* (Albright *et al.*, 2007), *Pliosaurus almanzaensis* (O'Gorman *et al.*, 2018), *Stenorhynchosaurus munozi* (Páramo-Fonseca *et al.*, 2019), *Megacephalosaurus eulerti* (Schumacher *et al.*, 2013), and probably *Pliosaurus patagonicus* (Gasparini & O'Gorman, 2014). Even if removal of the pyrite incrustationduring preparation process has destroyed part of the outermost bone layers, the tip of dentary appears rounded and does not form a flat anteroventral surface, unlike in *Pliosaurus rossicus* (Halstead, 1971), *Acostasaurus pavachoquensis* (Gómez-Pérez & Noè, 2017), and, to a lesser extent, *Kronosaurus–Eiectus* (Holland, 2018). A ventral symphysial keel is absent, as in all brachaucheniines (Schumacher *et al.*, 2013; Benson & Druckenmiller, 2014; Fischer *et al.*, 2015; Páramo-Fonseca *et al.*, 2016, 2018). Such a structure is also said to be absent in *Pliosaurus almanzaensis* (O'Gorman *et al.*, 2018) but a raised platform appears present instead and phylogenetic character 114 was thus scored as present by Fischer et al. (2020). A ventral keel has been described in *Kronosaurus–Eiectus* (Holland, 2018), but this structure rather appears as a faint paired ridge that diverge distally (V.F., pers. obs. on QM F10113), thus possibly not homologous with the keel seen in Middle – Late Jurassic thalassophoneans. The dentary forms a subtle dorsal expansion with larger teeth at the level of the premaxilla-maxilla suture, where a diastema is present in some Jurassic thalassophoneans (Druckenmiller & Russell, 2008; Ketchum & Benson, 2022). Posteriorly, the dentary becomes transversely compressed to form a sheet that covers the lateral surface of the mandible; its posterior termination is crenulated, forked, and located at the level of the coronoid, but clearly not as bifurcated in *Kronosaurus–Eiectus* (Holland, 2018). The dentary covers a part of the lateral and dorsal surface of the coronoid eminence, as in early pliosaurids (*Marmornectes candrewi*, *Peloneustes philarchus*) (Ketchum & Benson, 2011a,b) and unlike in *Megacephalosaurus eulerti*, *Acostasaurus pavachoquensis*, and *Kronosaurus–Eiectus* (Schumacher *et al.*, 2013; Gómez-Pérez & Noè, 2017; Holland, 2018).

Splenial. The splenial makes an extensive contribution to the symphysis, tapering anteriorly over 265 mm from the posterior end of the symphysis, reaching to the level of the 8th or 9th dental alveolus, thus 49.5% of the total symphysial length (Fig. 3). This is a much larger contribution than in other thalassophoneans (Noè, 2001; Gómez-Pérez & Noè, 2017; Holland, 2018; Páramo-Fonseca *et al.*, 2019). The ventral surface of the splenial in the symphysial region is mediolaterally broad, with a rounded cross-section. The ventral exposure of the splenial extends posteriorly way past mid-mandible, up to the level of the orbit. This exposure is thus much more extensive than in *Acostasaurus pavachoquensis* (Gómez-Pérez & Noè, 2017) and *Stenorhynchosaurus munozi* (Páramo-Fonseca *et al.*, 2019) where the ventral exposure of the splenial ends anterior to mid-mandible length. The ventral exposure of the splenial reaches mid-mandible length in *Kronosaurus–Eiectus* (Holland, 2018).

Angular. The angular is visible in lateral view (Figs 2, 3). It emerges laterally from under the posteroventral ramus of the dentary, at the level of the anterior margin of the orbit, thus much more posteriorly than in *Stenorhynchosaurus munozi*, and *Sachisaurus vitae* (Páramo-Fonseca *et al.*, 2018, 2019). The angular otherwise forms the ventral portion of the posterior half of the mandible, and participates to the retroarticular process. Its sutures with the surangular and articular are obscured by preparation and pyrite incrustation.

Surangular. Deep longitudinal ridges and furrows texture the surangular on its dorsal and dorsomedial surfaces, where it forms a major portion of the coronoid eminence (Fig. 3). This eminence is low compared to many Jurassic thalassophoneans such as *Pliosaurus kevani* (Benson *et al.*, 2013) and resembles the condition seen in other brachaucheniines (Holland, 2018; Páramo-Fonseca *et al.*, 2019), with the possible exception of *Acostasaurus pavachoquensis* (Gómez-Pérez & Noè, 2017). The dorsal surface of the surangular is mediolaterally expanded posterior to the coronoid eminence (Ketchum & Benson, 2010, 2011b), as in other thalassophoneans. As in some species of *Pliosaurus* and possibly *Kronosaurus–Eiectus*, this plateau faces slightly dorsolaterally (Benson *et al.*, 2013; Holland, 2018). The surangular fossa faces dorsolaterally, another similarity with some species of *Pliosaurus* (Benson *et al.*, 2013), that might also be present in *Kronosaurus–Eiectus* (Holland, 2018).

Retroarticular process and glenoid. The retroarticular process is formed by the fused angular, articular, and surangular. Its median anteroposterior length is 85 mm, and subequal to the length of the glenoid, unlike in *Pliosaurus brachyspondylus* (Taylor & Cruickshank, 1993) and *Anguanax zignoi* (Cau & Fanti, 2014), in which the glenoid appears much shorter anteroposteriorly than the retroarticular process. The long axis of the retroarticular process is posteromedially inturned relative to the long axis of the mandible (Fig. 3), a brachaucheniine feature (Williston, 1907; Schumacher & Martin, 2015; Gómez-Pérez & Noè, 2017; Noè & Gómez-Pérez, 2022) that is also possibly present but in a less conspicuous manner in *Pliosaurus almanzaensis* (O'Gorman *et*

al., 2018). In lateral view, it is clear that the retroarticular process extends approximately horizontally. The dorsal surface of the retroarticular process is dorsomedially inclined and saddle-shaped. The posterior end of the retroarticular process is not expanded mediolaterally, unlike in *Pliosaurus kevani* (Benson *et al.*, 2013) and possibly *Acostasaurus pavachoquensis* (Gómez-Pérez & Noè, 2017). As in other thalassophoneans, the glenoid is inclined to face dorsomedially (Andrews, 1913; Taylor & Cruickshank, 1993; Benson *et al.*, 2013; Gómez-Pérez & Noè, 2017; O'Gorman *et al.*, 2018). A broad sulcus separates the ventral margin of the angular from the ventral part of the glenoid.

Articular. The articular forms a saddle covering the dorsomedian surface of the mandible posterior to the coronoid plateau (Fig. 3). The articular cannot be thoroughly described because of imperfect preservation and anatomical connection with the quadrate. The articular forms a short anterior process, embaying the posterior part of the prearticular.

Dentition. The teeth of *Luskhan itilensis* are small for a pliosaurid of that size (basal diameter of the third dentary tooth crown = 22 mm compared to a skull length of 1585 mm). A slight variation in tooth size is present along the jaw: the largest teeth of the upper jaw are located on the anterior part of the maxilla, where the maxilla slightly expands ventrally. The largest dentary teeth are present at the level of the anteroventral end of the premaxilla-maxilla suture, where the dentary is slightly raised dorsally. However, there is no evidence for expanded caniniform teeth in *Luskhan itilensis*, unlike in many other pliosaurids such as *Peloneustes philarchus* (Ketchum & Benson, 2011b), *Liopleurodon ferox* (Andrews, 1913), *Pliosaurus* spp. (Sassoon *et al.*, 2012; Benson *et al.*, 2013; Gasparini & O'Gorman, 2014), *Sachicasaurus vitae* (Páramo-Fonseca *et al.*, 2018), *Kronosaurus–Eiectus* (White, 1935; McHenry, 2009; Holland, 2018), *Monquirasaurus boyacensis* (Noè & Gómez-Pérez, 2022), and possibly *Acostasaurus pavachoquensis* (based on the variation in the diameter of tooth alveoli along the dentary; Gómez-Pérez & Noè, 2017). This condition is thus similar to *Marmornectes candrewi* (Ketchum & Benson, 2011a), *Stenorhynchosaurus munozi* (Páramo-Fonseca *et al.*, 2016, 2019), *Brachauchenius lucasi* (Albright *et al.*, 2007; Schumacher *et al.*, 2013), and *Megacephalosaurus eulerti* (Schumacher *et al.*, 2013; Madzia *et al.*, 2018).

All teeth were damaged during extraction and preparation; however, the first right dentary tooth shows a somewhat rounded but still trihedral cross-section; photos taken during preparation of the specimen indicate that carinae were present at least on the labial surface (Fig. 7). *Makhaira rossica* and many species of *Pliosaurus* (Benson *et al.*, 2013; Arkhangelsky & Zverkov, 2015; Fischer *et al.*, 2015; Madzia *et al.*, 2018; O'Gorman *et al.*, 2018; Zverkov *et al.*, 2018) have trihedral teeth, while sub-trihedral teeth have been described in *Pliosaurus kevani* (Benson *et al.*, 2013), *Stenorhynchosaurus munozi* (Páramo-Fonseca *et al.*, 2019) and conical ones in *Sachicasaurus vitae*, *Monquirasaurus boyacensis, Acostasaurus pavachoquensis*, and middle Cretaceous (Aptian–Turonian) brachaucheniines (Madzia, 2016; Gómez-

Pérez & Noè, 2017; Páramo-Fonseca *et al.*, 2018; Zverkov *et al.*, 2018; Noè & Gómez-Pérez, 2022). Very fine, widely spaced, longitudinal ridges also ornament the distal and labial surfaces of the mesial-most crowns. The thinness and wide space between these ridges contrast with the condition seen in *Acostasaurus pavachoquensis*, and middle Cretaceous brachaucheniines such as *Megacephalosaurus eulerti*, *Kronosaurus–Eiectus*, and the nomen dubium '*Polyptychodon interruptus*' (Owen, 1841; Fischer *et al.*, 2016; Madzia, 2016; Gómez-Pérez & Noè, 2017; Madzia *et al.*, 2018; Zverkov *et al.*, 2018; McCurry *et al.*, 2019; Noè & Gómez-Pérez, 2022).

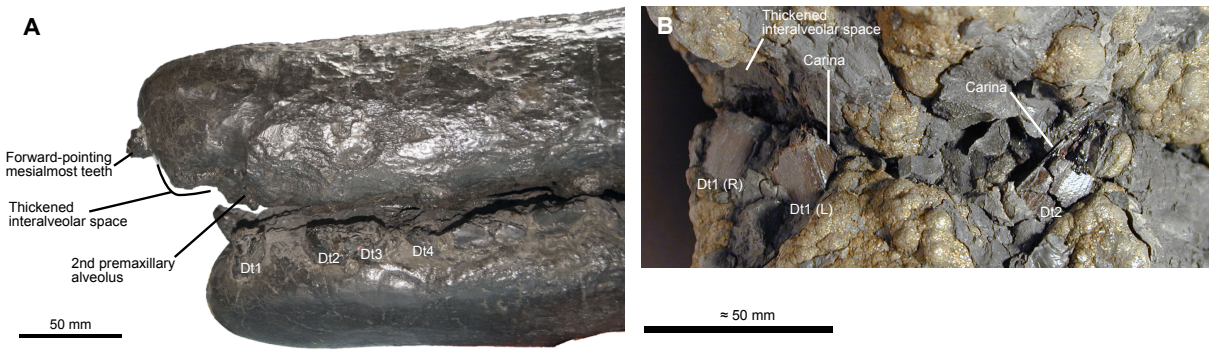

Figure 7. **Teeth of the holotype of *Luskhan itilensis* (YKM 68344/1_262)**. A, tip of the snout in left lateral view. B, picture taken during the preparation stage showing that the mesialmost dentary teeth possessed at least one carina.

Atlas-axis. The atlas-axis is preserved in articulation with the skull (Figs. 1, 6, 8). It is anteroposteriorly short (98 mm) relative to its mediolateral width (108 mm) and dorsoventral height (103 mm), similar to the situation in some thalassophoneans, such as *Liopleurodon ferox*, *Simolestes vorax*, *Pliosaurus* spp., *Kronosaurus–Eiectus*, and *Eardasaurus powelli* (Andrews, 1913; McHenry, 2009; Ketchum & Benson, 2022) and unlike in *Peloneustes philarchus*, '*Pliosaurus*' *andrewsi*, and *Stenorhynchosaurus munozi* (Andrews, 1913; Páramo-Fonseca *et al.*, 2019) where the atlas-axis is anteroposteriorly longer. The bases of the atlantal neural arches are preserved. They expand significantly ventromedially and posteroventrally, possibly contacting one another on the ventral floor of the neural canal, excluding or at least strongly reducing the contribution of the odontoid (=atlantal centrum) to the neural canal. This does not occur in other pliosaurids such as *Marmornectes candrewi* and *Peloneustes philarchus* (Linder, 1913; Ketchum & Benson, 2011a), and is at present autapomophic for *Luskhan itilensis* within pliosaurids; a similar condition is however seen in the early xenopsarian *Brancasaurus brancai* (Wegner, 1914; Sachs, Hornung, & Kear, 2016). The atlantal intercentrum is large, longer than the axis (55 mm vs. 43 mm) in anteroposterior length. This is similar to that of *Eardasaurus powelli* (Ketchum & Benson, 2022) and unlike the situation in many other plesiosaurians, including *Peloneustes philarchus* (Linder, 1913) and *Marmornectes candrewi* (Ketchum & Benson, 2011a), in which the anteroposterior length of the atlantal intercentrum is similar to that of the axis, or shorter. The ventral and anteroventral surfaces of the atlantal intercentrum are strongly convex, and the anterior portion of a narrow, triangular ventral keel is present on the ventral surface posteriorly. Facets on the lateral surface of the odontoid that are continuous with the posteroventral edge of the atlantal intercentrum suggest that the atlantal and axial intercentra contacted each other ventrally, excluding the odontoid from the ventral surface of the atlas-axis complex, as in *Marmornectes candrewi* (Ketchum & Benson, 2011a) and Jurassic thalassophoneans (Andrews, 1913; Ketchum & Benson, 2011a). The axial intercentrum is absent but its gross morphology can be inferred from the extensive facets on the other elements of the atlas-axis. The axial intercentrum is also strongly developed, reducing the posteroventral exposure of the axis to a thin, transversely oriented ridge, 11 mm in anteroposterior thickness. The axial intercentrum extends far dorsally, indenting the anteroventral margin of the axial rib facet, and giving it a 'V'-shaped outline in lateral view (Fig. 8).

There is no evidence for a rib-like posteroventral process on the odontoid, which has a smooth, concave lateral surface. The axial centrum possesses a single-headed rib facet (Fig. 8) which is a character common to all known brachaucheniines (Benson & Druckenmiller, 2014: character 143; Páramo-Fonseca *et al.*, 2018). A thin, but prominent ridge extends approximately dorsally from the rib facet, along the lateral surface of the axial centrum. This ridge is oriented dorsoventrally on the right side and is slightly inclined anteroventrally on the left side. A similar dorsoventral ridge is present in *Pliosaurus irgisensis* (N.G.Z., pers. obs. on the holotype PIN No 426).

Cervical vertebrae. The neck and first three pectorals are preserved in near anatomical connection (Fig. 8). The cervical series is complete and its total count (including the atlas and the axis) is 15, which is intermediate between that seen in *Pliosaurus* (18 cervicals; (Tarlo, 1959b)) and that seen in *Brachauchenius* (12 cervicals; (Williston, 1907)). The first centrum in which the transverse process contributes to at least one-quarter of the rib facet was considered to be the first pectoral centrum (sensu Seeley, 1869). The transverse process of the preceding vertebra to the first pectoral just contacts the rib facet and this centrum thus counted as a cervical. A narrow and prominent ridge, similar to that of the axis, extends dorsally from the rib facet to the neural arch facet on the lateral surface of the centrum. This ridge is most prominent in the four anteriormost centra after the atlas-axis complex. Unlike in the axis, this ridge is oriented strictly vertically on both sides. This ridge become broader and less prominent in more posterior centra but is present on all cervicals. The cervical rib facets are located just ventral to mid-height (Fig. 9), similar to those in *Stenorhynchosaurus munozi* (Páramo-Fonseca *et al.*, 2016), *Brachauchenius lucasi* (Albright *et al.*, 2007) and *Kronosaurus–Eiectus* (Benson & Druckenmiller, 2014); this differs from the ventromedially located cervical rib facets of other plesiosaurians, and was found to be a synapomorphy of Brachaucheniinae by Benson & Druckenmiller (2014). The cervical rib facets of *Luskhan itilensis* differ from those of *Brachauchenius lucasi* (Albright *et al.*, 2007) in being strongly concave and only weakly raised from the lateral surface of the centrum. These facets are single (i.e. not divided into two facets by a horizontal groove) as in other brachaucheniines (Benson & Druckenmiller, 2014) with the possible exception of *Acostasaurus pavachoquensis* (Gómez-Pérez, 2008). Well-developed, paired foramina are present on the ventral surfaces of all cervical centra, unlike in *Stenorhynchosaurus munozi*, *Kronosaurus–Eiectus*, and *Brachauchenius lucasi* (Williston, 1907; McHenry, 2009; Páramo-Fonseca *et al.*, 2016). Cervical centra possess a broad and prominent ventral lip extending from their anterior margin (Fig. 9), as in many pliosaurids (Tarlo, 1960). However, in *Luskhan itilensis*, this lip protrudes far anteroventrally in anterior cervicals, giving the cervical a wave-like shape in ventral view, unlike in other pliosaurids (Williston, 1907; Albright *et al.*, 2007; Ketchum & Benson, 2011a). This condition is most prominent in the 3rd cervical centrum, in which the lip is developed as a long concavo-convex tongue-like process that extends anteriorly to mid-length of the axis. The anterodorsal surface of the tongue-like process of the third cervical centrum is strongly concave, perhaps engulfing a small intercentrum.

The cervical neural arches are dorsoventrally tall and disarticulated from their corresponding centra. We interpret a small, disarticulated neural arch as belonging to an anterior cervical vertebra. This neural spine is transversely compressed and slightly transversely constricted at its base, as seen in anterior or posterior view. The ventral articular surface for the centrum is composed of two oblique flat facets in the anterior cervical neural arch. This gives them a weakly ‘V’-shaped outline in lateral view. Mid cervical neural spines are larger and more robust, forming a straight, thick process that thickens transversely on its dorsal end. This articular surface is gently concave in these more posterior cervical neural arches. The zygapophyseal facets are flat,

oriented horizontally and diverge anterolaterally such that they are separated from the midline along their entire lengths, whereas postzygapophyses are located close to each other (Fig. 9), as in *Stenorhynchosaurus munozi* (Páramo-Fonseca *et al.*, 2019). In Middle to Late Jurassic thalassophonean pliosaurids, the zygapophyseal surfaces – on the contrary – as wide as the width of the centrum. The neural spines are strongly offset posteriorly, having their mid-point located at the intercentral margin. The dorsal margin of the middle cervical neural spines is also slightly expanded laterally, giving them a rectangular cross-section with a concave dorsal surface. Mid cervical neural spines are taller (125–130 mm) than the dorsoventral diameter of the corresponding centrum (~92 mm).

The shape of the centra changes throughout the vertebral column, becoming increasingly long with respect to their dorsoventral height (Figs. 8, 9): the 3rd and 4th cervical centra are strongly anteroposteriorly compressed with a ratio of as high as 2.49 in the 3rd cervical centrum. The remainder of the cervicals have values slightly above 2.0 and the pectoral and anterior dorsal regions marks a rapid decrease of the height/length ratio close to 1.2, which stays stable up to the caudal region, included.

Pectoral, dorsal, and sacral vertebrae. Three pectoral, at least twenty dorsal, and at least two (but likely five) sacral vertebrae are preserved. The exact number of sacrals is indeed difficult to precise in the absence of well-preserved neural arches and ribs. The pectoral centra have thick transverse processes with a semi-circular cross-section and a posterior concave surface, while those on the anterior dorsal vertebrae are elongated, with concave anterior and posterior surfaces. Posterior dorsal transverse processes are dorsoventrally compressed, but only a few are preserved in the holotype of *Luskhan itilensis*. Paired foramina are present on the ventral surfaces of the third pectoral and all the dorsal centra where this trait is unambiguously assessable (Fig. 9). The floor of the neural canal, on the dorsal surface of the centrum, is pierced by numerous foramina that of variable size from 0.5 to 1 mm in diameter; this feature cannot be evaluated in pectorals due to the presence of crushed neural arches on that surface. Sacral centra have a slightly hexagonal outline in anteroposterior view; the ventral surface seems flatter than in *Peloneustes philarchus* (Linder, 1913). The lateral margins of the floor of the neural canal have a laterally-oriented concavity. Neural arches are not fused to their corresponding centra, which might indicate osteological immaturity (Brown, 1981), although even some very large specimens of pliosaurids show evidence of features that have sometimes been linked to osteological immaturity (McHenry, 2009; Noè & Gómez-Pérez, 2022), and might thus not be reliable for pliosaurids (Benson *et al.*, 2013; Zverkov & Pervushov, 2020). Dorsal neural arches are high: the base of the transverse processes is located dorsally to the mid-height of the neural canal (they are level with the neural canal in Jurassic thalassophoneans; (Benson & Druckenmiller, 2014)) (Fig. 9). The prezygapophyses face dorsally, and so are oriented broadly horizontally, although their articular surfaces are slightly concave mediolaterally.

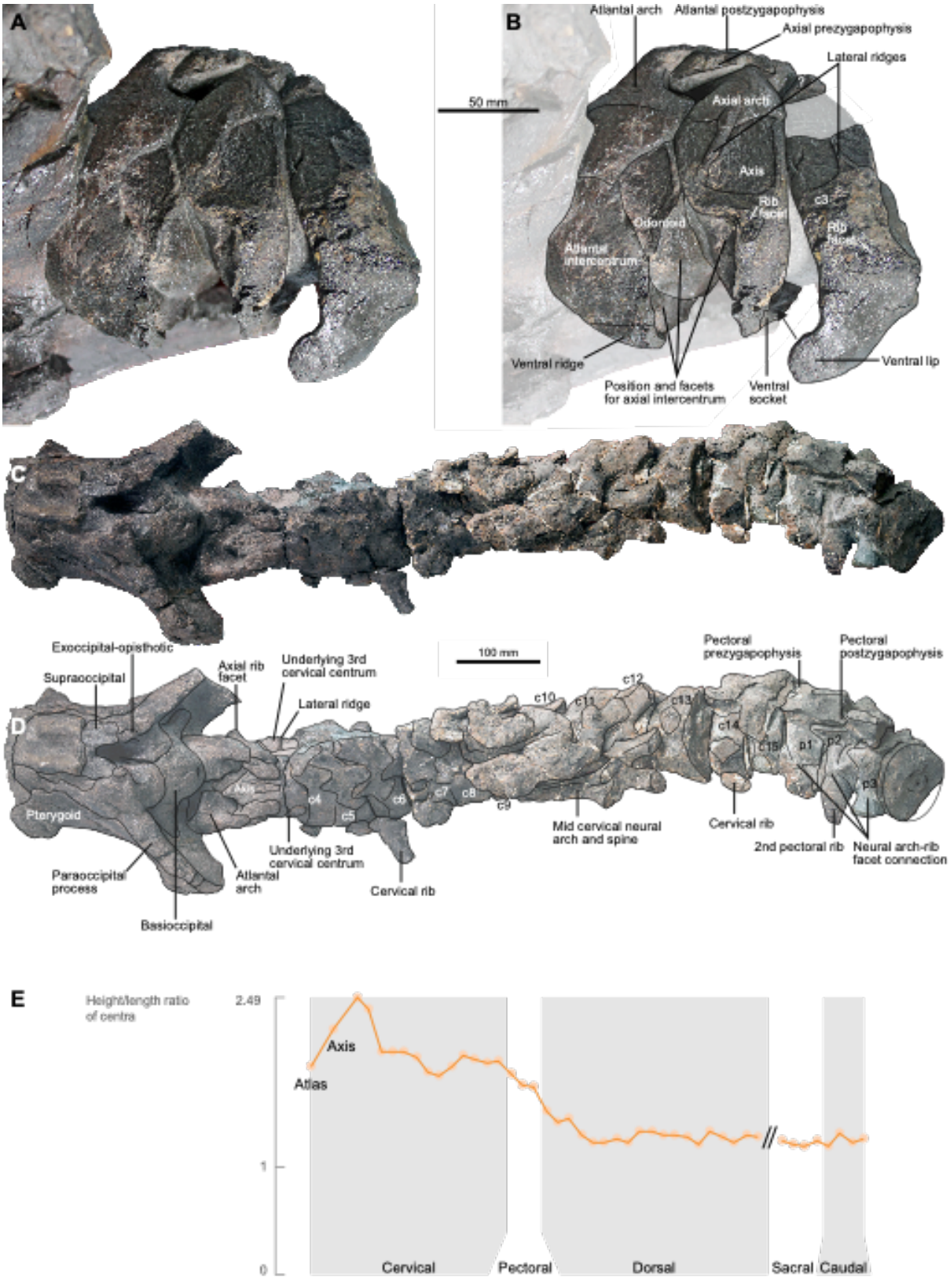

Figure 8. **Cervical region and centrum proportions of the holotype of *Luskhan itilensis* (YKM 68344/1_262)**. A–B, photographs and interpretation of the atlas-axis complex in left lateral view. C–D, photographs and interpretation of the cervical and pectoral regions, in dorsal view. E, evolution of the height/length ratio along the entire preserved vertebral column. Abbreviations: c, cervical; p, pectoral.

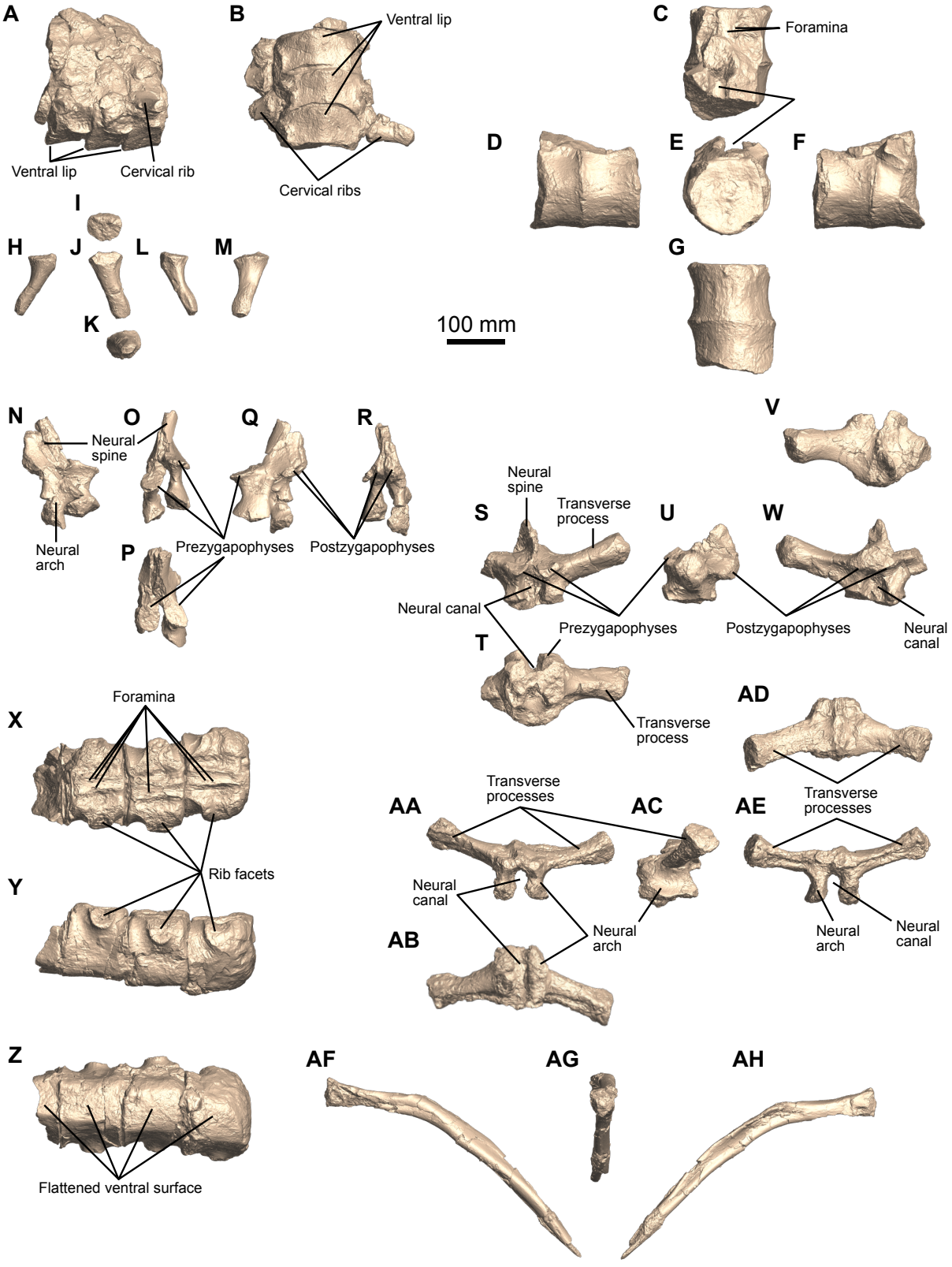

Figure 9. **Axial skeleton of the holotype of *Luskhan itilensis* (YKM 68344/1_262) based on high-resolution 3D models**. A, B anterior cervical vertebrae in left lateral (A) and ventral (B) views. C–G dorsal centra in dorsal (C), left lateral (D), anterior (E), right lateral (F), and ventral (G) views. H–M right cervical rib in anterior (H), proximal (I), ventral (J), distal (K), posterior (L), and dorsal (M) views. N–R cervical neural arc in right lateral (N), anterior (O), dorsal (P), left lateral (Q), and posterior (R) views. S–W dorsal neural arc in anterior (S), ventral (T), left lateral (U), dorsal (V), and posterior (W) views. X–Z, caudal centra in dorsal (X), left lateral (Y), and ventral (Z) views. AA–AE more posterior dorsal neural

arc in anterior (AA), ventral (AB), left lateral (AC), dorsal (AD), and posterior (AE) views. AF–AH, dorsal rib in anterior (AF), proximal (AG), and posterior (AH) views.

Caudal vertebrae. At least five caudal centra are preserved. Anterior caudal centra have a flat ventral surface, with paired subcentral foramina (Fig. 9), possibly similar to the 'triangular' condition described in *Sachicasaurus vitae* (Páramo-Fonseca *et al.*, 2018). The lateral surface bears a protruding, semi-oval caudal rib facet situated within the top half of the centrum and that is confluent with the neural arch facet, as is mostly seen in pliosaurids and polycotylids (e.g. Andrews, 1913; Sato, 2005). Ventrally to that facet, the lateral surface of the anterior caudals is slightly concave. As in dorsal centra, the floor of the neural canal is pierced by numerous foramina of varying size; the lateral margins of this surface are concave. Posterior caudals are poorly preserved in the holotype of *Luskhan itilensis*: only one partial centrum from this region is preserved. It has a squared cross-section, with flattened ventral and lateral surfaces. Large semioval chevron facets are present, contacting the anterior margin of the centrum.

Ribs. Most cervical ribs are single-headed (Fig. 9), even though at least one cervical rib is bicapitate, as evidenced by the articular surface of a cervical rib still connected to its rib facet in one posterior cervical vertebra. This slight polymorphism along the cervical series provides a potential explanation for the seemingly volatile nature of this character. Indeed, a double-headed cervical rib preserved in the holotype of *Megacephalosaurus eulerti* (FHSM VP-32; (Schumacher *et al.*, 2013)), as well as in the 3rd cervical centrum of the holotype of *Monquirisaruus boyacensis* (Gomez 2001 in Hampe, 2005), while other brachaucheniine specimens besides *Acostasaurus pavachoquensis* (Gómez-Pérez, 2008), have single-headed cervical rib facets (Albright *et al.*, 2007; Schumacher *et al.*, 2013; Páramo-Fonseca *et al.*, 2016). Nevertheless, all cervical rib facets are simple and oval in *Luskhan itilensis*, not paired or '8'-shaped. The cervical and pectoral ribs are simple and conical; their long axis is directed posterolaterally. They lack an anterior process and their diameter rapidly decreases lateral to their articular facet – a feature commonly found in brachaucheniines which differ from the distally-expanding cervical ribs seen in more basal pliosaurids (Andrews, 1913). The surface of the cervical ribs is textured by numerous longitudinal ridges.

The proximal portions of the dorsal ribs are rod-like. A small dorsal process is present where the rib initiates its ventral bending. There, the rib shaft becomes strongly flattened and slightly anteroposteriorly expanded, with a deep posteroventral longitudinal sulcus. More distally, the rib becomes again rod-like thin and anteroposteriorly compressed distally. The dorsal ribs appear slender, as in *Stenorhynchosaurus munozi* (Páramo-Fonseca *et al.*, 2016, 2019), and unlike in *Monquirasaurus boyacencis* (Hampe, 1992; Noè & Gómez-Pérez, 2022) and *Sachicasaurus vitae* (Páramo-Fonseca *et al.*, 2018). One proximal portion of a sacral rib is preserved. It possesses two articular facets forming an obtuse angle, one facing dorsomedially for articulation with the neural arch and one facing ventromedially for

articulation with the sacral centrum. This shape appears similar to that reported in *Peloneustes philarchus* by Linder (1913), although it is probably more common among pliosaurids.

Coracoid. The coracoid is large; the coracoid/scapula length ratio equals 2.3 (Fig. 10), which is similar to that of *Kronosaurus–Eiectus* (ca. 2.5) but higher than in *Stenorhynchosaurus munozi* (<2) (McHenry, 2009; Páramo-Fonseca *et al.*, 2016). The anteromedial process of the coracoid is short, triangular, and points ventrally, forming a 90° angle with the main surface of the coracoid. This process is markedly inflected ventrally and is unlikely to have contacted the ventral process of the scapula. While a strong curvature of the coracoid symphysis is often present in well-preserved specimens (Andrews, 1913) (N.G.Z., pers. obs. on NHMUK PV R3897 and R2437), *Luskhan itilensis* appears peculiar in having an anteromedial process that clearly points anteroventrally rather than anteriorly. The median intercoracoid facet is strongly thickened dorsally compared to well-known Jurassic forms (e.g. Andrews, 1913), but this might be due to different taphonomical settings. Ventrally, the symphysis is concave and no mediolaterally oriented buttress is present, unlike in the dorsal surface. The coracoids are inclined dorsolaterally from the midline, so their ventral surfaces face clearly ventrolaterally, as in *Peloneustes philarchus* (Andrews, 1913). The shape of the posterior part of the coracoid suggests the absence of a tight osseous intercoracoid contact posteriorly. The posterolateral cornu extends further laterally than the glenoid, as in *Peloneustes philarchus* (Andrews, 1913; Ketchum & Benson, 2011a), *Simolestes vorax* (Andrews, 1913; Ketchum & Benson, 2011a), *Brachauchenius lucasi* (Albright *et al.*, 2007) and probably as in *Stenorhynchosaurus munozi* (Páramo-Fonseca *et al.*, 2016), and unlike in *Anguanax zignoi* and *Sachicasaurus vitae* (Cau & Fanti, 2014; Páramo-Fonseca *et al.*, 2018). The posterior margin of the coracoid is straight in dorsal view and oriented posterolaterally.

Scapula. The scapula is triradiate, comprising a dorsal blade and ventral plate made up of a posterior, glenoid ramus, and anterior ramus (Fig. 10). The dorsal surface of the ventral plate is smooth and slightly convex while the ventral surface is mostly flat medially. This surface is separated from the base of the dorsal process by a long, strongly thickened lateral ridge that is ventrally and medially bowed. This ridge merges with the lateral edge of the scapula anterolaterally. The posterior process of the scapula is strongly thickened; the glenoid facet is semi-circular, with a flat ventral margin and the coracoid facet is triangular. The long axes of these facets form a 120° angle, similar to what is seen in other pliosaurids (e.g. Andrews, 1913; Noè & Gómez-Pérez, 2022). The anterior ramus is sheet-like and strongly medially expanded giving it a fan shape; it does not contact the anteromedial part of the coracoid. The dorsal blade is longer than the ventral process and is not posteriorly inclined. Therefore, it forms a 90° angle with the ventral surface of the scapula when seen in lateral view, as in *Pliosaurus* and unlike in earlier pliosaurids, where it is posterodorsally inclined (Andrews, 1913; Tarlo, 1960). The shaft of the dorsal blade has a teardrop shaped cross-section, with a thickened posterior edge. The dorsal process is fan-shaped, with

a dorsal end that is strongly expanded anteroposteriorly. In other thalassophoneans, the dorsal process is either fan-shaped but less so than in *Luskhan itilensis*, such as in *Pliosaurus rossicus* (Halstead, 1971) or expands in anteroposterior length dorsally without creating a fan-shaped, as in *Peloneustes philarchus*, *Liopleurodon ferox*, *Simolestes vorax*, and *Sachicasaurus vitae* (Andrews, 1913; Tarlo, 1960; Páramo-Fonseca *et al.*, 2018).

Forefin. The right forefin, including the humerus, is 1495 mm long proximodistally, just 10 cm shorter than the mandible. This is likely similar to *Stenorhynchosaurus munozi* (Páramo-Fonseca *et al.*, 2016) and this condition seems to contrast with the absolutely and relatively larger skull of *Monquisaurus boyacensis* (Hampe, 1992; Noè & Gómez-Pérez, 2022), although the forefin of the only-known specimen might not be complete.

Humerus. The humerus is shorter proximodistally than the femur, as in other pliosaurids (e.g. Andrews, 1913; Hampe, 1992, 2005; McHenry, 2009; O'Gorman *et al.*, 2018). The humerus is robust (proximodistal length/anteroposterior length at mid-shaft = 3.9) and distally expanded (anteroposterior distal length/anteroposterior shaft length = 1.78-1.9), this is similar in proportions to those of *Liopleurodon ferox* and *Sachicasaurus vitae* (Andrews, 1913; Páramo-Fonseca *et al.*, 2018), and differs from the narrower shaft seen in *Monquirasaurus boyacensis* (Noè & Gómez-Pérez, 2022) and from the thicker shaft with less marked distal expansion of *Pliosaurus* spp.(Tarlo, 1960; O'Gorman *et al.*, 2018). The distal expansion is present both anteriorly and posteriorly and starts just distal to mid-length; the posterior expansion forms an extensive sheet-like flange demarcated from the body of the humerus by dorsal and ventral longitudinal concavities (Fig. 10), unlike in other pliosaurids (Andrews, 1913; O'Gorman *et al.*, 2018; Páramo-Fonseca *et al.*, 2018; Noè & Gómez-Pérez, 2022). The humerus is straight: its capitulum and its shaft are not deflected posteriorly, as seen in some Early Jurassic plesiosaurians (Smith & Dyke, 2008), or anteriorly to form the 'sigmoid' humerus that is seen in some xenopsarians (e.g. Welles, 1962; Schumacher, 2007). Both the anterior and posterior edges are flat to slightly concave medially and gently convex more distally. Unusually, the dorsal tuberosity is well-developed, being higher than the ventral expansion of the humeral head. Extensive muscle scars are present on dorsal surface of the left humerus, over 10 cm distal to the capitulum and on the anterior surface, at mid-length. Long, slightly convex and marginally tapering facets are present; their long axes are oblique to one another, forming an angle of approximately 150°. There are no supernumerary epipodial facets.

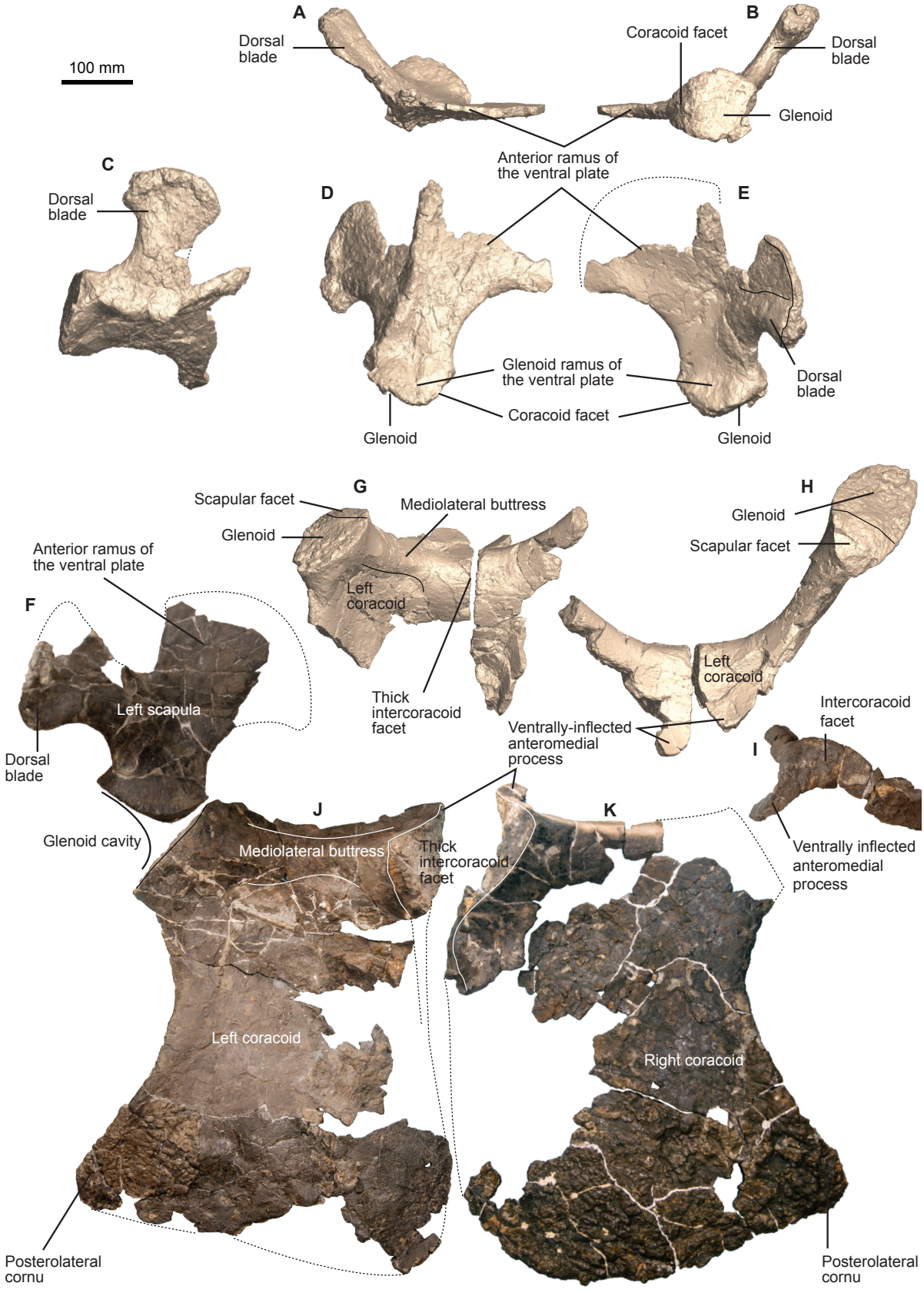

Figure 10. **Scapular girdle of the holotype of *Luskhan itilensis* (YKM 68344/1_262)**. A–E, right scapula in anterior (A), posterior (B), lateral (C), ventral (D), and dorsal (E) views. F, left scapula in dorsal view. G–I, anterior coracoids in dorsal (G), anterior (H), and medial (I) views. J, left coracoid in dorsal view. K, right coracoid in dorsal view.

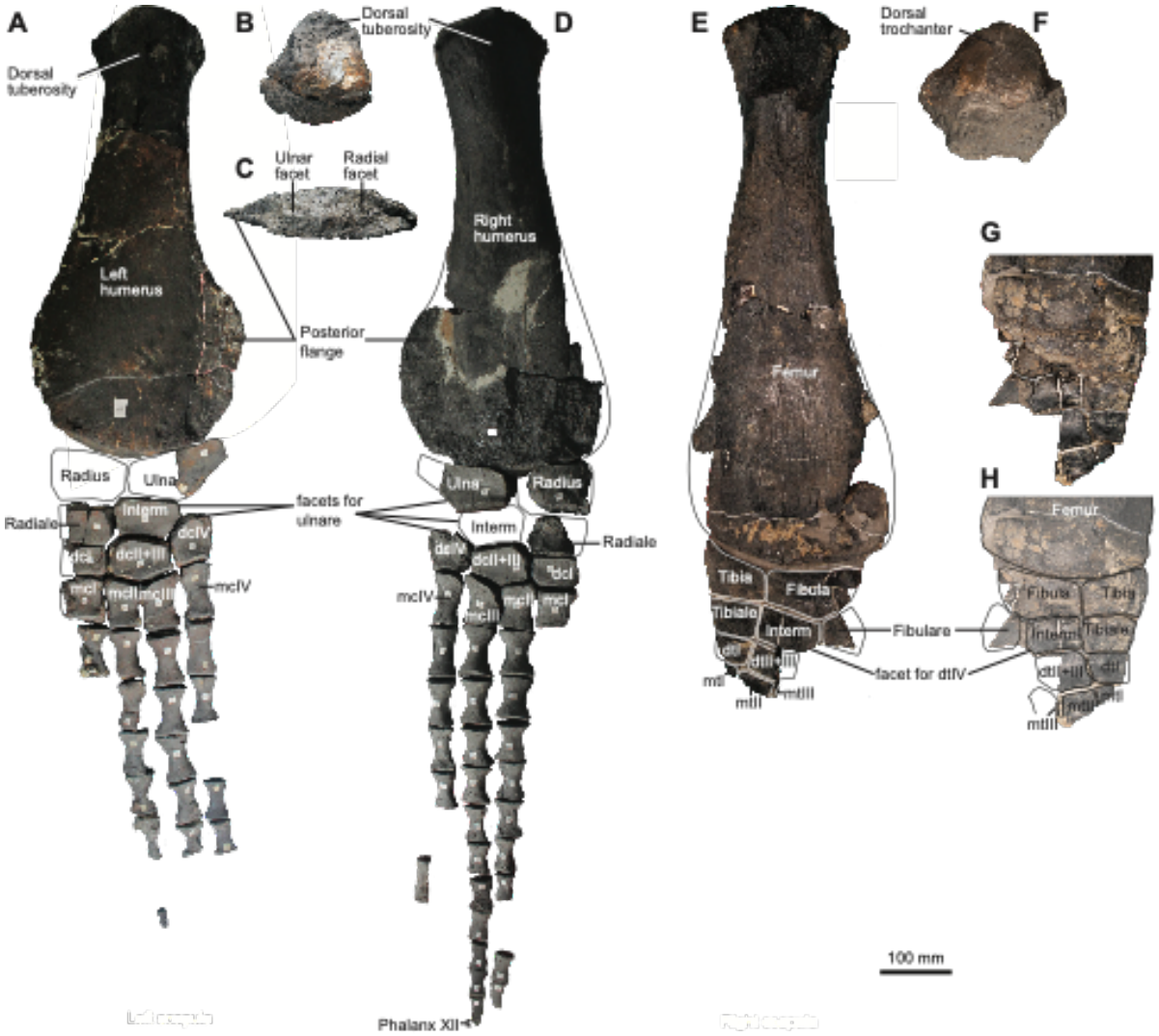

Figure 11. **Limbs the holotype of *Luskhan itilensis* (YKM 68344/1_262)**. A, left forefin in dorsal view. B–C, right humerus in proximal (B) and distal (C) views. D, right forefin in dorsal view. E–F, right hind fin in ventral (E) and proximal (F) views. G–H, photographs and interpretation of the right hind fin in dorsal view.

Epipodium and autopodium. The proximal elements are polygonal and tightly fitting (Fig. 11). The epipodial row appears proximodistally short (radius length/width = 1.42), as in derived polycotylids, and unlike in other pliosaurids (Ketchum & Benson, 2011a) with the possible exception of *Stenorhynchosaurus munozi* (Páramo-Fonseca *et al.*, 2016) and *Pliosaurus* spp. (Tarlo, 1960; O'Gorman *et al.*, 2018). The radius of the holotype of *Luskhan itilensis* is incompletely preserved, but its straight and dorsoventrally thin anterior surface suggests that no anterior accessory epipodial element was present. The preserved left intermedium indicates that a small intermedium facet was present on the radius. The facets on the humerus and the proximal shape of the intermedium indicate the ulna was 1.17 times longer than the radius. The ulna is strongly waisted in posterior view and the spatium interosseum is absent, unlike in Middle and Late Jurassic pliosaurids (Andrews, 1913; Tarlo, 1960). The intermedium is also proximodistally short (L/W = 1.63). Its ulnar facet is very long and faces nearly proximally. The radiale possesses a facet for the distal carpal II+III, and this latter element is wider and nearly as long as the intermedium. No evidence for a metacarpal V contact is found on the posterior facet of the distal carpal IV. Additionally, the fifth digit appears completely absent in both forefins; it is unclear whether this absence is an additional genuine feature of *Luskhan itilensis* or is taphonomic, given the fact that the fifth digit can be quite slender and reduced in derived thalassophoneans (Schumacher & Everhart, 2005; see also Páramo-Fonseca *et al.*, 2016 for potential preservation bias of a fifth digit in thalassophoneans). The distal carpal I possesses a small facet for the metacarpal II and the distal carpal IV possesses a minute facet for metacarpal III. Phalanges (even the distalmost ones) are proximodistally short, being only 1.28 to 1.59 times wide as they are long; only some phalanges of the 4th digit reach a slightly higher ratio of 1.78. The longest digit preserved (digit III of the right forefin) possesses 12 phalanges and appears complete. Eleven phalanges are recorded in *Stenorhynchosaurus munozi* (Páramo-Fonseca *et al.*, 2016).

Pubis. Pubes are poorly preserved and have been fragmented into dozens of centimetric elements; and most of the bone margins appears missing. The pubis becomes sheet-like immediately anteromedial to the acetabulum (Fig. 12).

Ischium. The right ischium is preserved. It is elongated (length/width = 615/330 = 1.86). Its symphysis is wave-shaped in medial view, with a dorsal expansion (Fig. 12), although less conspicuous than in the coracoid. The anterior edge is weakly embayed in dorsal view and the anteromedial process appears small. Although its anterior extent cannot be precisely determined, its lateral edge suggests that a 'median pelvic bar' was absent, unlike in *Simolestes vorax* (Andrews, 1913). The pubic facet is semicircular and faces ventroanterolaterally. The iliac facet is triangular and faces dorsolaterally.

Ilium. The right ilium is preserved but its dorsal blade is incomplete. The anterior margin of its dorsal extremity forms a ca. 50° angle with the long axis of the pelvic

shaft end, giving the ilium a markedly expanded dorsal process (this is inferred from broken preserved morphology) (Fig. 12). The dorsal process of the ilium appears anteroposteriorly shorter in *Peloneustes philarchus*, *Simolestes vorax* (Andrews, 1913) and slightly shorter in *Pliosaurus* cf. *kevani* (Tarlo, 1957, described as a scapula; 1959b; Benson *et al.*, 2013)). The shaft is oval in cross-section. The ischial facet is triangular, oblique to the long axis of the ilium, and appears larger than the acetabular facet. The anterior surface of the ilium is strongly curved in lateral view, becoming parallel with the acetabular facet.

Femur. The femur is proximodistally longer than the humerus (mean femur proximodistal length/mean humerus proximodistal length = 1.27) (Fig. 11), as is often the case in pliosaurids that are more derived than *Hauffiosaurus* (e.g. see data in Fischer *et al.*, 2020). Its shape is also different: it is proportionally longer in comparison to its width than is the humerus, but with a slightly smaller distal expansion (proximodistal length/anteroposterior shaft length = 4.54 to 4.86; anteroposterior distal length/anteroposterior shaft length ≥1.72) (none of the distal ends of the femora are complete but shape of the femur can be estimated by combining the left and right femora). This condition resembles that of *Stenorhynchosaurus munozi* (Páramo-Fonseca *et al.*, 2016). On the contrary, the femur exhibits a more pronounced distal expansion than the humerus in *Sachicasaurus vitae* and *Monquirasaurus boyacensis* (Páramo-Fonseca *et al.*, 2018; Noè & Gómez-Pérez, 2022). Contrary to the humerus, the distal portion of the femur seemingly lacks a sheet-like posterior lamella. The femur is straight: its capitulum and its shaft are not deflected anteriorly or posteriorly. Medially, the anterior surface is concave and the posterior surface is saddle-shaped. The dorsal trochanter is semioval in cross-section and slightly shorter anteroposteriorly than the capitulum as a whole. The femur forms two distal facets, forming an angle of approximately 160°. As in the humerus, the distal end of the femur extends further posteriorly than the epipodium, but we found no evidence for an extrazeugopodial element, as the posterior surface of the fibula is thin and edge-like.

Epipodium and autopodium. The fibula is 1.34 times anteroposteriorly longer than the tibia. The epipodial elements are proximodistally shortened (tibia L/W: 1.26; fibula L/W: 1.57; intermedium L/W: 1.55) and polygonal, forming a tightly fitting mosaic. A spatium interosseum between the tibia and the fibula is absent unlike in other pliosaurids for which this part of the anatomy is adequately known (Andrews, 1913; Tarlo, 1960). Unusually, the intermedium is located directly distal to the fibula, and thus possesses only one flat proximal surface, giving this element a rectangular shape (Fig. 11). The tibiale is trapezoidal and articulates distally solely with the distal tarsal I; this condition is also seen in *Stenorhynchosaurus munozi* (Páramo-Fonseca *et al.*, 2016). The intermedium articulates distally with the distal tarsal II+III; a small posterodistal facet is present for the distal tarsal IV, unlike in other pliosaurids, where the distal facets of the intermedium are subequal in length (Andrews, 1913; Tarlo, 1960). The distal tarsal II+III is anteroposteriorly enlarged, which has a size similar to

that of the intermedium, as in *Stenorhynchosaurus munozi* (Páramo-Fonseca *et al.*, 2016). A single complete proximal hind fin phalanx is preserved; its W/L ratio is 1.32.

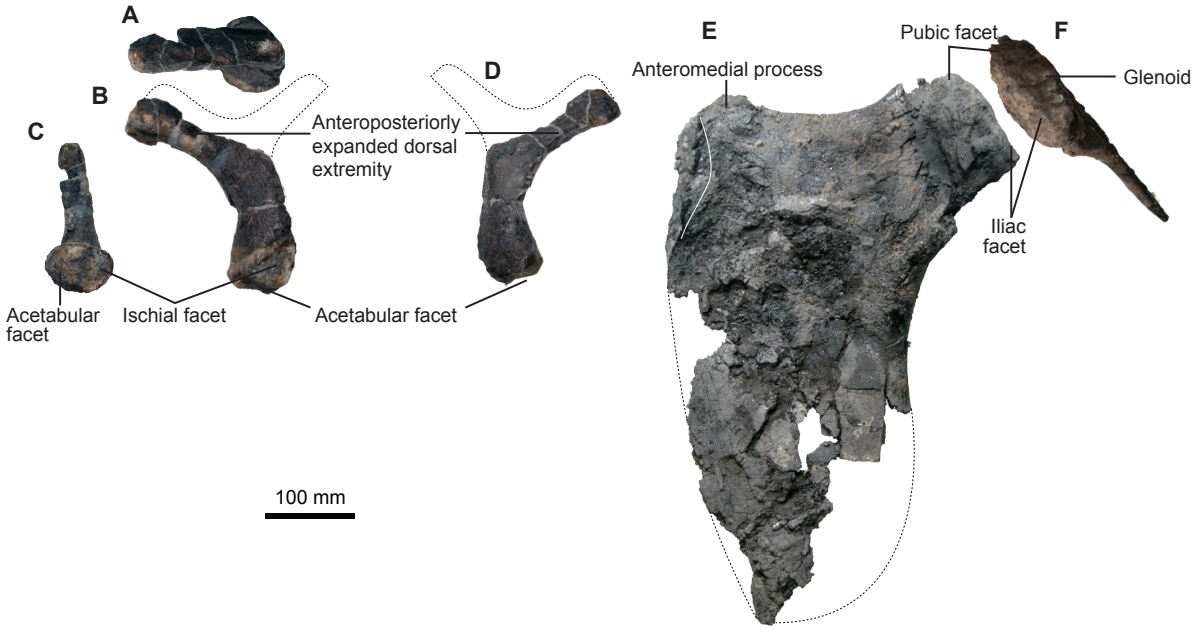

Figure 12. **Pelvic girdle of the holotype of *Luskhan itilensis* (YKM 68344/1_262)**. A–D, left ilium in dorsal (A), medial (B), ventral (C), and lateral (D) views, along with a reconstruction of the possible extent of the dorsal blade (pitted line). E–F, right ilium in dorsal (E) and anterolateral (F) views.

RESULTS

Maximum parsimony inference of phylogeny. Fischer et al. (2020) used implied weighting to generate a phylogenetic hypothesis, for analyses of evolutionary convergence. However, a single concavity constant was used (k = 3). Here, we test for changes in topology by using increasing values of k (6, 9, 12), thereby progressively reducing the penalty applied on homoplastic features. This results in a slight loss of resolution within *Pliosaurus*, as well as the inclusion of *Gallardosaurus iturraldei* into the clade of *Pliosaurus*, where it groups with *Pliosaurus kevani* in k = 9 and k = 12 iterations (Figs. 13, S1, S2, S3). brachaucheniines form a large polytomy in all our maximum parsimony analyses, and systematically incorporates the Late Jurassic taxon *Pliosaurus patagonicus*, which is recovered as closely related to *Luskhan itilensis* (Figs. 13, S1, S2, S3). The Early Cretaceous taxa from Columbia *Sachicasaurus vitae* and *Stenorhynchosaurus munozi* also form a clade and *Acostasaurus pavachoquensis* is systematically recovered as the most basal brachaucheniine, as in the Bayesian inference produced by Madzia & Cau (2020).

Bayesian inference of topology and rates of morphological evolution. The general topology is similar to previous maximum parsimony analyses of the Benson & Druckenmiller (2014) dataset, where the radiation of Thalassophonea is initially marked by stepwise evolution (*Peloneustes philarchus*, "*Pliosaurus*" *andrewsi*, *Simolestes vorax*, *Liopleurodon ferox*, *Gallardosaurus iturraldei*) that then leads to a split: the '*Pliosaurus* clade' (here recovered as large polytomy) and Brachaucheniinae (Benson & Druckenmiller, 2014; Fischer *et al.*, 2015, 2017; O'Gorman *et al.*, 2018; Morgan & O'Keefe, 2019; Páramo-Fonseca *et al.*, 2019; Madzia & Cau, 2020) (Figs. 14, S4). However, we recover *Pliosaurus patagonicus* as the sister lineage to all Cretaceous pliosaurids. By definition (see Benson & Druckenmiller, 2014), both maximum parsimony and Bayesian inference recover this late Jurassic taxa as a brachaucheniine pliosaurid, although in a more basal position than within the maximum parsimony framework. *Luskhan itilensis*, then *Makhaira rossica* + *Stenorynchosaurus munozi* are recovered as early brachaucheniines, while *Acostasaurus pavachoquensis* and *Sachicasaurus vitae* are the successive sister lineages to the 'traditional', middle Cretaceous brachaucheniines (*Monquirasaurus*, *Kronosaurus*, *Brachauchenius*, *Megacephalosaurus*, and '*Polyptychodon'*). This slightly differs from the results of our maximum parsimony analyses and Madzia & Cau (2020), where *Acostasaurus pavachoquensis* is the most basal brachaucheniine.

The early radiation of Thalassophonea and the nodes directly leading to it are marked by clearly elevated rates of morphological evolution (Fig. 14); these high rates are sustained during the entire Middle Jurassic, a period marked by rapid turnovers among marine reptiles (Fischer, Weis, & Thuy, 2021). Both the radiation of *Pliosaurus* during the Late Jurassic and the diversification of Brachaucheniinae during the Cretaceous are characterised by slow rates of morphological evolution, corroborating the results of a previous attempt (Madzia & Cau, 2020). This suggests that the recently described Early Cretaceous brachaucheniines (*Makhaira rossica*, *Luskhan itlensis*,

Stenorhynchosaurus munozi, *Acostasaurus pavachoquensis*, *Sachicasaurus vitae*) have effectively bisected the long branch that previously connected *Liopleurodon*-like forms of the Middle Jurassic to the Middle Cretaceous brachaucheniines. One exception is the lineage of *Sachicasaurus vitae*, which briefly records the highest rates of evolution among Pliosauridae. The morphological differences between *Acostasaurus pavachoquensis*, *Sachicasaurus vitae*, and *Kronosaurus–Eiectus* might explain the poor resolution within Brachaucheniinae (and the basal placement of *Acostasaurus*) in a maximum parsimony framework, while a relaxed morphological clock rather considers *Sachicasaurus vitae* as an exception in an otherwise slowly evolving grade. In Madzia & Cau (2020), high rates were briefly recorded at a similar time (earliest Cretaceous), but slightly closer to the origin of Brachaucheniinae (more specifically the branches leading to *Luskhan itilensis* and *Stenorhynchosaurus munozi*). This difference might be explained by alteration of some brachaucheniine character scores by Fischer al. (2020), and incorporated in the present analyses. The evolution of middle Cretaceous brachaucheniines is marked by a sustained period of slow rates of morphological innovation (see also Madzia & Cau, 2020), up to their extinction at the end of the Turonian (Schumacher, 2011).

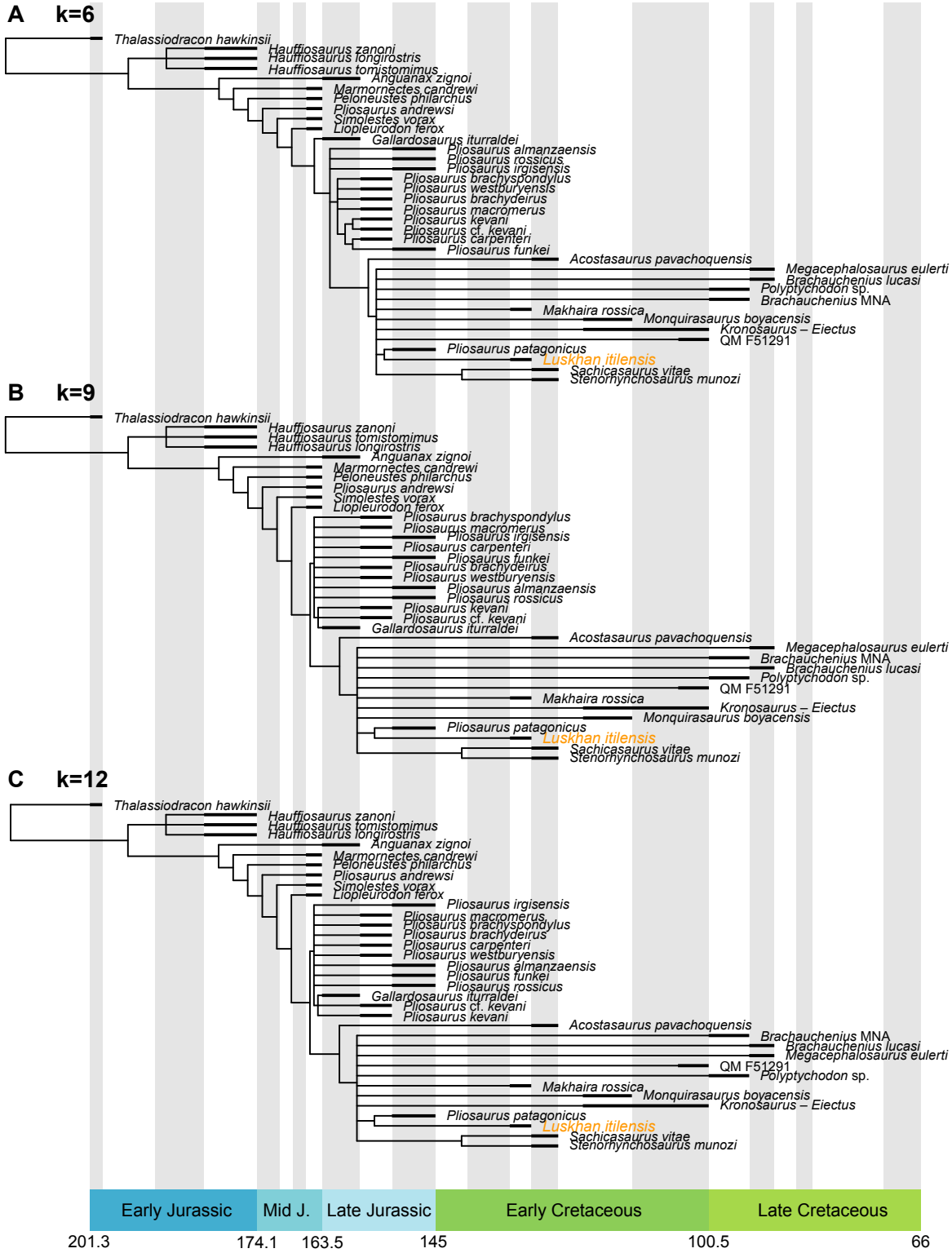

Figure 13. **Phylogenetic relationships among Pliosauridae**. A–C, temporally scaled strict consensus trees depicting the phylogenetic relationships of Pliosauridae in an implied weighting maximum parsimony framework, with increasing concavity constants (k), which progressively reduces the penality applied to homoplasic characters. A, k=6. B, k=9. C, k=12.

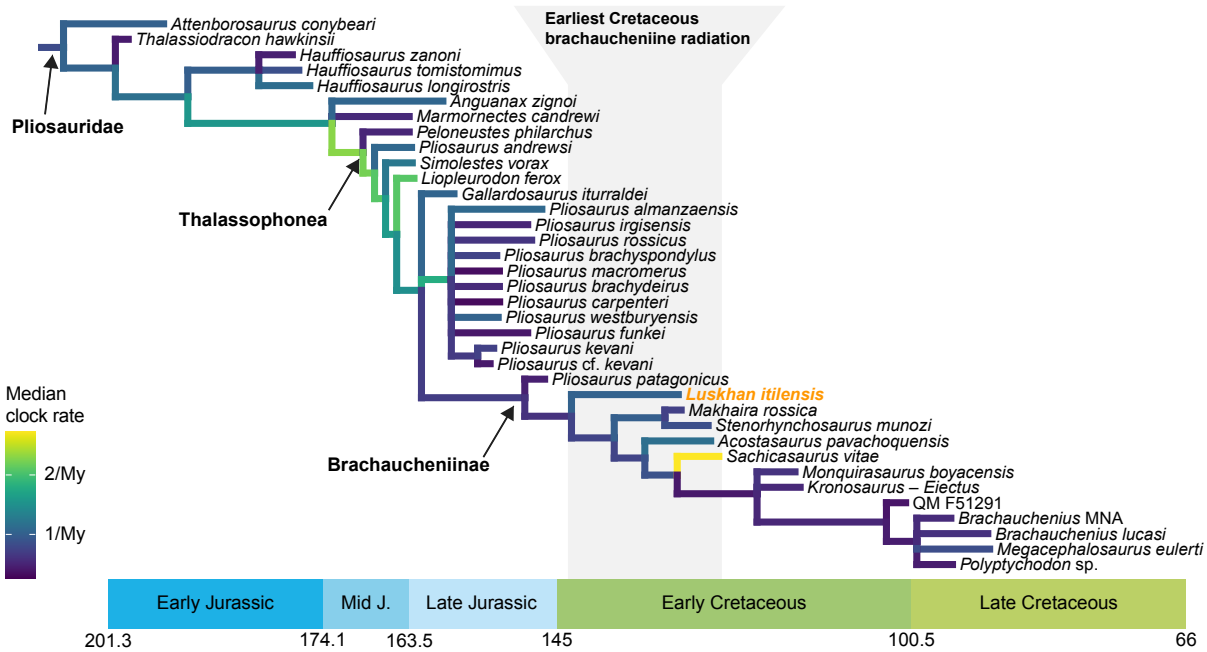

Figure 14. **Phylogenetic relationships among Pliosauridae**. Extended majority consensus tree ("allcompat") obtained by a relaxed morphoclock Bayesian inference. Each branch is coloured according to its medial clock rate from the posterior distribution.

DISCUSSION

Luskhan itilensis is notably characterized by a unique combination of plesiomorphic and derived features within thalassophoneans, bisecting the long temporal and morphological branch separating mid-Cretaceous brachaucheniines from Late Jurassic pliosaurids. Far more unexpected were the several autapomorphic features of *Luskhan itilensis*, which significantly depart from morphology of thalassophoneans (Fischer *et al.*, 2017). One of the most striking of these features are the forward-pointing first premaxillary teeth that appear to be supported posteriorly by thickened interalveolar bone of the premaxilla, forcing the presence of a thickened diastema between the 1st and the 2nd premaxillary alveoli (Figs. 2, 3, 7). We reject the hypothesis that this feature is an artefact of taphonomic deformation, given the excellent state of preservation of the holotype specimen. The hypothesis of a pathology appears difficult to assess in a population of one individual, besides the fact that this trait is fully symmetrical and did seemingly not modify the dorsal and lateral parts of the rostrum. The absence of a similar structure on the dentary likely precludes a direct involvement in food procurement and processing, unlike in the several marine and terrestrial taxa bearing procumbent teeth that probably permit easier catch of small prey items (e.g. Chatterjee & Small, 1989). “[F]orwardly oriented” mesial dentary teeth have been described in another pliosaurid, *Pliosaurus patagonicus* (Gasparini & O’Gorman, 2014: 276). However, these alveoli are broken off; because plesiosaurian alveoli are internally curved (e.g. Sassoon, Foffa, & Marek, 2015), it is presently impossible to conclude whether *Pliosaurus patagonicus* had forward pointing teeth or not. The mesialmost teeth of the mosasaurid *Prognathodon solvayi* and the ophthalmosaurid ichthyosaurian *Pervushovisaurus campylodon* can be slightly oriented anteriorly (Lingham-Soliar & Nolf, 1989; Fischer, 2016, respectively) (Fig. 15) but, again, this condition does not resemble that of *Luskhan itilensis*.

Some tusked ziphiid cetaceans (beaked whales) bear some similarities with *Luskhan itilensis*, having procumbent mesial teeth (Fig. 15) as well as thickened rostral bones (e.g. Bianucci *et al.*, 2016). The ziphiid *Tasmacetus* is especially interesting, possessing two forward-pointing mesialmost teeth (albeit on the dentary), and which are positioned anterior to an elongated diastema. Gut content suggest that this dental adaptation is not linked to a particular diet (Best *et al.*, 2014) and hence is a poor predictor of ecological niche. However, these supplementary bone deposits in the anterior part of the rostrum are hypothesised to play a role in absorbing stresses resulting from use of the anteriorly-oriented tusks during male fights (Lambert, Bianucci, & Post, 2010). Squalodontid odontocetes also have forward pointing mesial tooth crowns that are supported by elongated, horizontally inclined roots (e.g. Fordyce, 1994) (Figure 15), yet lack the thickened interalveolar bone and the diastema seen in *Luskhan itilensis* (e.g. Rothausen, 1968). In both ziphiids and squalodontids, these features are thought to be associated with visual display and, for some extant ziphiids, male fights, leaving a series of scars on the body of old adult males (Heyning, 1984). The ‘tusks’ of *Luskhan itilensis* could thus have served a similar function given the morphological similarity. Caution is however needed, as evidence for visual display

and male-male behavioural interactions are exceedingly rare among Mesozoic marine reptiles (Zammit & Kear, 2011).

The enlarged atlantal and axis intercentra and the broad atlas-axis neural arch of *Luskhan itilensis* form, altogether, a thick layer of bone nearly completely wrapping the odontoid and the axis. Moreover, the cervical centra of *Luskhan itilensis* posses an elongated anteroventral processes inserting into a wide groove situated in the anterior centrum. This process is very large on the 3rd cervical centrum and progressively decreases in size in more posterior centra. Such a feature (the cervical 'lip') is present in other pliosaurids (Tarlo, 1960), but much smaller. Mechanically, all these cervical features would likely lock the anterior part of the neck, preventing movement in this region and, possibly, help absorb shocks and pressure. Neck stiffening has evolved several times in marine amniotes, being found in ichthyosaurians (through fusion (Broili, 1907; McGowan & Motani, 2003; Maxwell & Kear, 2010) and/or undulating margins (Fischer *et al.*, 2012)) and cetaceans (through extensive fusion (e.g. VanBuren & Evans, 2016)) and is interpreted – in pelagic taxa – as an adaptation to high-speed swimming (Fish, 2000; McGowan & Motani, 2003; VanBuren & Evans, 2016). The long skull of *Luskhan itilensis* is clearly convergent with the supposedly fast swimming (Adams, 1997) polycotylid plesiosaurians (Fischer *et al.*, 2017, 2020). *Luskhan itilensis* also departs from the large headed morphology seen in all other thalassophoneans, having a mandibular/femur length = 1.81 while other thalassophoneans besides *Peloneustes philarchus* and *Simolestes vorax* have values from 2.0 to 2.73 (Fischer *et al.*, 2020). All these lines of evidence suggest that both the morphology and probable niche and behaviour of *Luskhan itilensis* strongly differed from those of other pliosaurids.

Nevertheless, our Bayesian inference results indicates that internal branches within Late Jurassic-Late Cretaceous pliosaurids have generally low rates of morphological evolution overall (Fig. 14). These rates represent the transition frequencies of cladistic characters rather than specifically the most functionally or ecologically relevant traits of species. Furthermore, they do not consider the multiple autapomorphies of *Luskhan itilensis* or other species. These low rates indicate, in general, that the recently described Early Cretaceous pliosaurids from Russia and Colombia have populated the gap that previously separated *Pliosaurus* from *Kronosaurus*, *Brachauchenius*, and *Megacephalosaurus*, presenting somewhat 'intermediate' combinations of character states, with only minimal occurrence of distinctive new morphotypes. The last pliosaurids record very low evolutionary rates (see also Madzia & Cau, 2020), large to very large sizes (Longman, 1930; Benson *et al.*, 2013; Zverkov & Pervushov, 2020), and a reduced range of craniodental morphologies (Fischer *et al.*, 2020) prior to their extinction, which presumably occurred at the end of the Turonian (Schumacher, 2011). This combination of selective extinctions strongly recalls the events associated with the Cenomanian extinction of ichthyosaurians (Fischer, 2016; Fischer *et al.*, 2016) and might be indicative of global restructuring of marine trophic webs at the beginning of the Late Cretaceous.

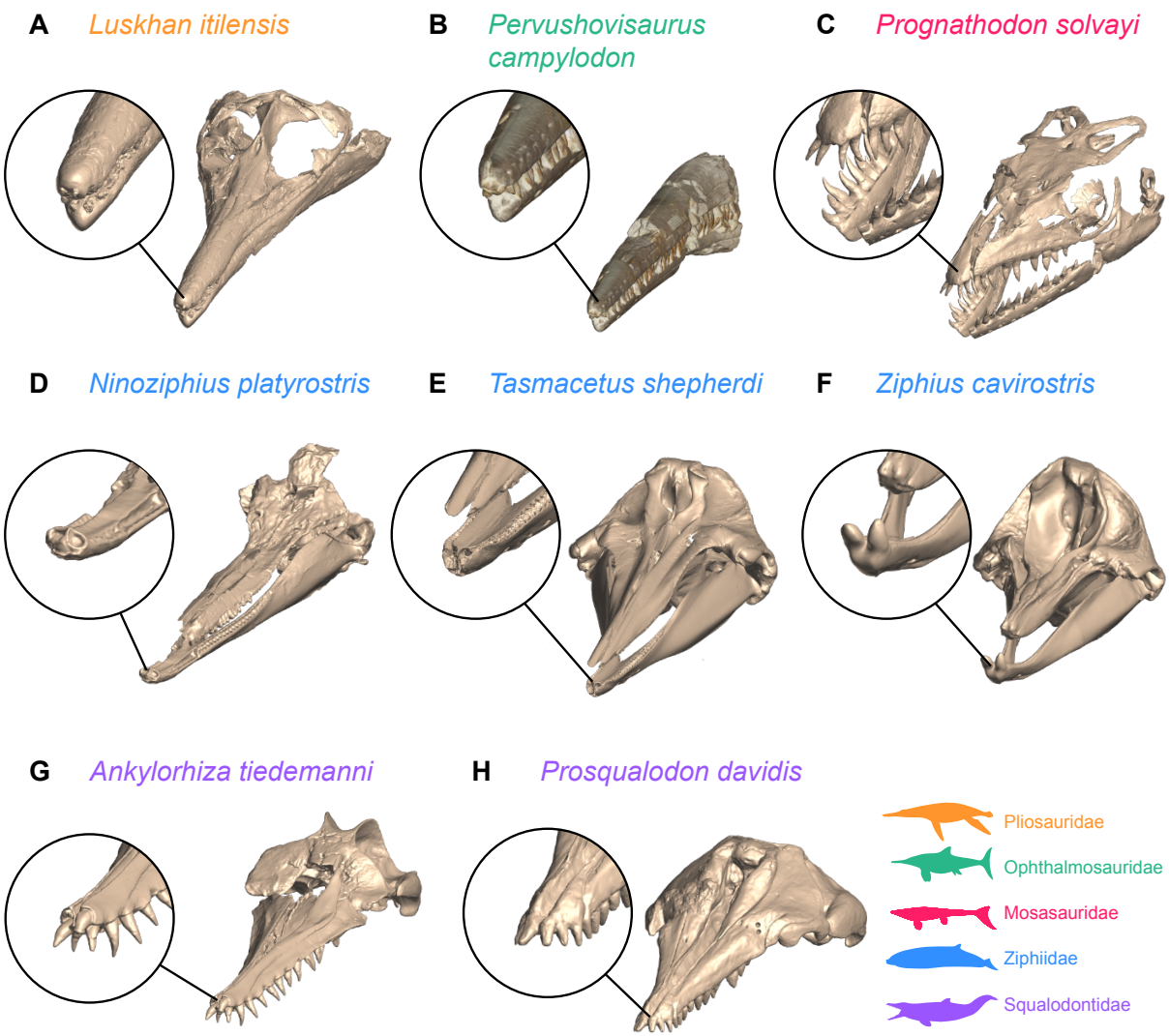

Figure 15. **Comparative cranial anatomy of raptorial marine amniote with procumbent mesialmost teeth**. All are high-resolution 3D models. A, *Luskhan itilensis* (YKM 68344/1_262). B, *Pervushovisaurus campylodon* (CAMSM B20671). C, *Prognathodon solvayi* (IRSNB R33b). D, *Ninoziphius platyrostris* (MNHN SAS 941). E, *Tasmacetus shepherdi* (USNM 484878). F, *Ziphius cavirostris* (NHMUK 1915.7.20.1). *Ankylorhiza tiedemanni* (CCNHM 103). H, *Prosqualodon davidis* (USNM 467596). Silhouettes: *Ziphius* by Chris Huh, from Phylopic (http://phylopic.org/image/7c1d06fb-2d6e-454d-b57b-a859d5dbdb9f/); *Squalodon* by Craig Hylke, from Phylopic (http://phylopic.org/image/95a73c63-e7c7-4e81-8e6d-592f647b07bc/), vectorised by V.F.; others by V.F.

CONCLUSIONS

Luskhan itilensis is a peculiar brachaucheniine thalassophonean from the Hauterivian of western Russia, documenting the 'Early Cretaceous gap' in pliosaurid evolution. Our thorough comparative description and high-precision 3D surface scans confirms the uniqueness of numerous traits of *Luskhan itilensis* such as the long, slender rostrum, forward-pointing mesial premaxillary teeth resembling the morphology seen in some ziphiid whales, hook-like processes on the squamosal, and ventrally-dipping anterior processes of the coracoids. Despite its unique phenotype and possible ecology, *Luskhan itilensis* forms a grade with a series of other Early Cretaceous pliosaurids that bisects the long branch separating middle Cretaceous brachaucheniines from their *Pliosaurus*-like ancestors. This, in turn, results in low morphological evolutionary rates during the entire Cretaceous history of pliosaurids, especially just prior to their extinction in the early Late Cretaceous.

AUTHOR CONTRIBUTIONS

V.F., R.B.J.B., N.G.Z., and M.S.A. designed the project and wrote the paper. I.M.S., G.N.U., N.G.Z., and M.S.A. prepared the specimen and gathered the stratigraphic and geological data. N.E.P. and V.F. scanned the specimens and processed the 3D data. V.F. ran the analyses. All authors significantly contributed to the manuscript.

ACKNOWLEDGEMENTS

We warmly thank the staff of YKM for their help. VF was supported by MIS Grant from the F.R.S.–FNRS (MIS F.4511.19). The work of NGZ is supported by the Geological Institute of RAS. NEP thanks Sergey Sukhovey (Artec 3D) for his advice and technical support in scanning and processing the 3D models and Ruslan Belyaev for his assistance in processing 3D models. We thank Vlad Konstantinov for his 3D reconstruction of the skeleton of *Luskhan itilensis* made for Undory Paleontological Museum, Rebecca Bennion, and Jamie MacLaren for providing 3D models of marine amniote skulls, and Hillary Ketchum for discussion and data. Finally, we thank the editor Maarten Christenhusz as well as BA Schumacher and anonymous colleagues who made this paper better by their thoughtful and sensible reviews.

REFERENCES

Adams DA. 1997. *Trinacromerum bonneri*, new species, last and fastest pliosaur of the Western Interior Seaway. *Texas Journal of Science* 49: 179–198.

Albright BL, Gillette DD, Titus AL. 2007. Plesiosaurs from the Upper Cretaceous (Cenomanian-Turonian) tropic shale of southern Utah, Part 1: New records of the pliosaur *Brachauchenius lucasi*. *Journal of Vertebrate Paleontology* 27: 41–58.

Andrews CW. 1913. *A descriptive catalogue of the Marine Reptiles of the Oxford Clay, part II* (T of the B Museum, Ed.). London: British Museum of Natural History.

Angst D, Bardet N. 2016. A new record of the pliosaur *Brachauchenius lucasi* Williston, 1903 (Reptilia: Sauropterygia) of Turonian (Late Cretaceous) age, Morocco. *Geological Magazine* 153: 449–459.

Arkhangelsky MS, Zverkov NG. 2015. A Valanginian ichthyosaur from Kirov region

(Russia) supporting the Jurassic-Cretaceous boundary crossing for ichthyosaurs. *The International Scientific Conference on the Jurassic / Cretaceous boundary. Sept. 7-13, Sarama, Russia*. Tolyatti, Russia: Kassandra, 15–20.
Bapst DW. 2012. paleotree: an R package for paleontological and phylogenetic analyses of evolution. *Methods in Ecology and Evolution* 3: 803–807.
Bell MA, Lloyd GT. 2015. strap : an R package for plotting phylogenies against stratigraphy and assessing their stratigraphic congruence. *Palaeontology* 58: 379–389.
Benson RBJ, Bates KT, Johnson MR, Withers PJ. 2011a. Cranial anatomy of *Thalassiodracon hawkinsii* (Reptilia, Plesiosauria) from the Early Jurassic of Somerset, United Kingdom. *Journal of Vertebrate Paleontology* 31: 562–574.
Benson RBJ, Butler RJ, Lindgren J, Smith AS. 2010. Mesozoic marine tetrapod diversity: mass extinctions and temporal heterogeneity in geological megabiases affecting the vertebrates. *Proceedings of the Royal Society B: Biological Sciences* 277: 829–834.
Benson RBJ, Druckenmiller PS. 2014. Faunal turnover of marine tetrapods during the Jurassic–Cretaceous transition. *Biological Reviews* 89: 1–23.
Benson RBJ, Evans M, Druckenmiller PS. 2012. High diversity, low disparity and small body size in plesiosaurs (Reptilia, Sauropterygia) from the Triassic–Jurassic boundary. *PLoS ONE* 7: e31838.
Benson RBJ, Evans M, Smith AS, Sassoon J, Moore-Faye S, Ketchum HF, Forrest R. 2013. A giant pliosaurid skull from the Late Jurassic of England. *PLoS ONE* 8: e65989.
Benson RBJ, Ketchum HF, Noè LF, Gómez-Pérez M. 2011b. New information on *Hauffiosaurus* (Reptilia, Plesiosauria) based on a new species from the Alum Shale member (Lower Toarcian: Lower Jurassic) of Yorkshire, UK. *Palaeontology* 54: 547–571.
Best PB, Smale MJ, Glass J, Herian K, Von Der Heyden S. 2014. Identification of stomach contents from a Shepherd's beaked whale Tasmacetus shepherdi stranded on Tristan da Cunha, South Atlantic. *Journal of the Marine Biological Association of the United Kingdom* 94: 1093–1097.
Bianucci G, Di Celma C, Urbina M, Lambert O. 2016. New beaked whales from the late Miocene of Peru and evidence for convergent evolution in stem and crown Ziphiidae (Cetacea, Odontoceti). *PeerJ* 4: e2479.
Blainville de HMD. 1835. Description de quelques espèces de reptiles de la Californie, précédée de l'analyse d'un système général d'Erpetologie et d'Amphibiologie. *Nouvelles annales du Muséum d'Histoire naturelle, Paris* 4: 233–296.
Broili F. 1907. Ein neuer *Ichthyosaurus* aus der norddeutschen Kreide. *Palaeontographica* 54: 139–162.
Brown D. 1981. The English Upper Jurassic Plesiosauroidea (Reptilia) and a review of the phylogeny and classification of the Plesiosauria. *Bulletin of the British Museum (Natural History) Geology* 35: 253–347.
Brown D, Vincent P, Bardet N. 2013. Osteological redescription of the skull of

Microcleidus homalospondylus (Sauropterygia, Plesiosauria) from the Lower Jurassic of England. *Journal of Paleontology* 87: 537–549.
Carpenter K. 1996. A review of short-necked plesiosaurs from the Cretaceous of the Western Interior, North America. *Neues Jahrbuch für Geologie und Paläontologie, Abhandlungen* 201: 259–287.
Cau A, Fanti F. 2014. A pliosaurid plesiosaurian from the Rosso Ammonitico Veronese Formation of Italy. *Acta Palaeontologica Polonica* 59: 643–650.
Chatterjee S, Small BJ. 1989. New plesiosaurs from the Upper Cretaceous of Antarctica. *Geological Society, London, Special Publications* 47: 197–215.
Druckenmiller PS, Russell AP. 2008. Skeletal anatomy of an exceptionally complete specimen of a new genus of plesiosaur from the Early Cretaceous (Early Albian) of northeastern Alberta, Canada. *Palaeontographica* 293: 1–33.
Fischer V. 2016. Taxonomy of *Platypterygius campylodon* and the diversity of the last ichthyosaurs. *PeerJ* 4: 1–21.
Fischer V, Arkhangelsky MS, Stenshin IM, Uspensky GN, Zverkov NG, Benson RBJ. 2015. Peculiar macrophagous adaptations in a new Cretaceous pliosaurid. *Royal Society Open Science* 2: 150552.
Fischer V, Bardet N, Benson RBJ, Arkhangelsky MS, Friedman M. 2016. Extinction of fish-shaped marine reptiles associated with reduced evolutionary rates and global environmental volatility. *Nature communications* 7: 1–11.
Fischer V, Benson RBJ, Druckenmiller PS, Ketchum HF, Bardet N. 2018. The evolutionary history of polycotylid plesiosaurians. *Royal Society Open Science* 5: 172177.
Fischer V, Benson RBJ, Zverkov NG, Soul LC, Arkhangelsky MS, Lambert O, Stenshin IM, Uspensky GN, Druckenmiller PS. 2017. Plasticity and convergence in the evolution of short-necked plesiosaurs. *Current Biology* 27: 1667–1676.
Fischer V, Maclaren JA, Soul LC, Bennion RF, Druckenmiller PS, Benson RBJ. 2020. The macroevolutionary landscape of short-necked plesiosaurians. *Scientific reports* 10: 16434.
Fischer V, Maisch MW, Naish D, Kosma R, Liston J, Joger U, Krüger FJ, Pardo Pérez J, Tainsh J, Appleby RM. 2012. New ophthalmosaurid ichthyosaurs from the European Lower Cretaceous demonstrate extensive ichthyosaur survival across the Jurassic-Cretaceous boundary. *PLoS ONE* 7: e29234.
Fischer V, Weis R, Thuy B. 2021. Refining the marine reptile turnover at the Early-Middle Jurassic transition. *PeerJ* 9: 1–45.
Fish FE. 2000. Biomechanics and Energetics in Aquatic and Semiaquatic Mammals: Platypus to Whale. *Physiological and Biochemical Zoology* 73: 683–698.
Fordyce RE. 1994. *Waipatia maerewhenua* New Genus and New Species (Waipatiidae, New Family), an Archaic Late Oligocene Dolphin (Cetacea: Odontoceti: Platanistoidea) from New Zealand. *Proceedings of the San Diego Society of Natural History*.147–176.
Gasparini Z. 2009. A new Oxfordian pliosaurid (Plesiosauria, Pliosauridae) in the Caribbean seaway. *Palaeontology* 52: 661–669.
Gasparini Z, O'Gorman JP. 2014. A New Species of *Pliosaurus* (Sauropterygia,

Plesiosauria) from the Upper Jurassic of Northwestern Patagonia, Argentina. *Ameghiniana* 51: 269–283.
Goloboff PA, Catalano SA. 2016. TNT version 1.5, including a full implementation of phylogenetic morphometrics. *Cladistics* 32: 221–238.
Goloboff PA, Torres A, Arias JS. 2018. Weighted parsimony outperforms other methods of phylogenetic inference under models appropriate for morphology. *Cladistics* 34: 407–437.
Gómez-Pérez M. 2008. The palaeobiology of an exceptionally preserved Colombian pliosaur (Sauropterygia : Plesiosauria). Unpublished thesis, University of Cambridge.
Gómez-Pérez M, Noè LF. 2017. Cranial anatomy of a new pliosaurid *Acostasaurus pavachoquensis* from the Lower Cretaceous of Colombia, South America. *Palaeontographica Abteilung A* 310: 5–42.
Halstead L. 1971. *Liopleurodon rossicus* (Novozhilov)–a pliosaur from the lower Volgian of the Moscow Basin. *Palaeontology* 14: 566–570.
Hampe O. 1992. Ein grosswüchsiger pliosauride (Reptilia, Plesiosauria) aus der Unterkreide (oberes Aptium) von Kolumbien. *Courier Forschungsintitut Senckenberg* 145: 1–32.
Hampe O. 2005. Considerations on a *Brachauchenius* skeleton (Pliosauroidea) from the lower Paja Formation (late Barremian) of Villa de Leyva area (Colombia). *Fossil record — Mitteilungen aus dem Museum dür Naturkunde in Berlin, Geowissenschaften* 8: 37–51.
Heyning JE. 1984. Functional morphology involved in intraspecific fighting of the beaked whale, Mesoplodon carlhubbsi. *Canadian journal of zoology* 62: 1645–1654.
Holland T. 2018. The mandible of *Kronosaurus queenslandicus* Longman, 1924 (Pliosauridae, Brachaucheniinae), from the Lower Cretaceous of Northwest Queensland, Australia. *Journal of Vertebrate Paleontology* e1511569: 1–12.
Kear BP. 2003. Cretaceous marine reptiles of Australia: a review of taxonomy and distribution. *Cretaceous Research* 24: 277–303.
Ketchum HF, Benson RBJ. 2010. Global interrelationships of Plesiosauria (Reptilia, Sauropterygia) and the pivotal role of taxon sampling in determining the outcome of phylogenetic analyses. *Biological Reviews* 85: 361–392.
Ketchum HF, Benson RBJ. 2011a. A new pliosaurid (Sauropterygia, Plesiosauria) from the Oxford Clay Formation (Middle Jurassic, Callovian) of England: evidence for a gracile, longirostrine grade of Early–Middle Jurassic pliosaurids. *Special Papers in Palaeontology* 86: 109–129.
Ketchum HF, Benson RBJ. 2011b. The cranial anatomy and taxonomy of *Peloneustes philarchus* (Sauropterygia, Pliosauridae) from the Peterborough Member (Callovian, Middle Jurassic) of the United Kingdom. *Palaeontology* 54: 639–665.
Ketchum H, Benson R. 2022. A new pliosaurid from the Oxford Clay Formation of Oxfordshire, UK. *Acta Palaeontologica Polonica* 67: 297–315.
Knutsen EM. 2012. A taxonomic revision of the genus *Pliosaurus* (Owen, 1841a) Owen, 1841b. *Norwegian Journal of Geology* 92: 259–276.
Lambert O, Bianucci G, Post K. 2010. Tusk-bearing beaked whales from the

Miocene of Peru: sexual dimorphism in fossil ziphiids? *Journal of Mammalogy* 91: 19–26.
Linder H. 1913. Beiträge zur Kenntnis der Plesiosaurier-Gattungen Peloneustes und Pliosaurus. *Geologische und Palæontologische Abhandlungen* 11: 339–409.
Lingham-Soliar T, Nolf D. 1989. The mosasaur *Prognathodon* from the Upper Cretaceous of Belgium (Reptilia, Mosasauridae). *Bulletin de l'Institut Royal des Sciences Naturelles de Belgique* 59: 137–190.
Longman HA. 1930. *Kronosaurus queenslandicus*. A gigantic Cretaceous pliosaur. *Memoirs of the Queensland Museum* 10: 1–7.
Madzia D. 2016. A reappraisal of *Polyptychodon* (Plesiosauria) from the Cretaceous of England. *PeerJ* 4: e1998.
Madzia D, Cau A. 2020. Estimating the evolutionary rates in mosasauroids and plesiosaurs : discussion of niche occupation in Late Cretaceous seas. *Peer* 8: 1–31.
Madzia D, Sachs S, Lindgren J. 2018. Morphological and phylogenetic aspects of the dentition of *Megacephalosaurus eulerti*, a pliosaurid from the Turonian of Kansas, USA, with remarks on the cranial anatomy of the taxon. *Geological Magazine*: 1–16.
Massare JA. 1987. Tooth morphology and prey preference of Mesozoic marine reptiles. *Journal of Vertebrate Paleontology* 7: 121–137.
Maxwell EE, Kear BP. 2010. Postcranial anatomy of *Platypterygius americanus* (Reptilia: Ichthyosauria) from the Cretaceous of Wyoming. *Journal of Vertebrate Paleontology* 30: 1059–1068.
McCurry MR, Evans AR, Fitzgerald EMG, McHenry CR, Bevitt J, Pyenson ND. 2019. The repeated evolution of dental apicobasal ridges in aquatic-feeding mammals and reptiles. *Biological Journal of the Linnean Society* 127: 245–259.
McGowan C, Motani R. 2003. *Part 8. Ichthyopterygia* (HD Sues, Ed.). München: Verlag Dr. Friedrich Pfeil.
McHenry CR. 2009. 'Devourer of Gods'. The palaeoecology of the Cretaceous pliosaur *Kronosaurus queenslandicus*. Unpublished thesis, University of Newcastle.
Morgan DJ, O'Keefe FR. 2019. The cranial osteology of two specimens of Dolichorhynchops bonneri (Plesiosauria, Polycotylidae) from the Campanian of South Dakota, and a cladistic analysis of the Polycotylidae. *Cretaceous Research* 96: 149–171.
Motani R, Jiang DY, Tintori A, Ji C, Huang JD. 2017. Pre- versus post-mass extinction divergence of mesozoic marine reptiles dictated by time-scale dependence of evolutionary rates. *Proceedings of the Royal Society B: Biological Sciences* 284.
Noè LF. 2001. A taxonomic and functional study of the Callovian (Middle Jurassic) Pliosauroidea (Reptilia, Sauropterygia). Unpublished thesis, University of Derby.
Noè LF, Gómez-Pérez M. 2022. Giant pliosaurids (Sauropterygia; Plesiosauria) from the Lower Cretaceous peri-Gondwanan seas of Colombia and Australia. *Cretaceous Research* 132.
Noè LF, Smith DTJ, Walton DI. 2004. A new species of Kimmeridgian pliosaur (Reptilia; Sauropterygia) and its bearing on the nomenclature of *Liopleurodon macromerus*. *Proceedings of the Geologists' Association* 115: 13–24.

O'Gorman JP, Gasparini Z, Spalletti LA. 2018. A new *Pliosaurus* species (Sauropterygia, Plesiosauria) from the Upper Jurassic of Patagonia: new insights on the Tithonian morphological disparity of mandibular symphyseal morphology. *Journal of Paleontology* 92: 240–253.
O'Keefe FR. 2001. A cladistic analysis and taxonomic revision of the Plesiosauria (Reptilia:Sauropterygia). *Acta Zoological Fennica* 213: 1–63.
Owen R. 1841. *Odontography; or, a treatise on the comparative anatomy of the teeth; their physiological relations, mode of developement, and microscopic structure, in the vertebrate animals*. London: Hippolyte Bailliere.
Paradis E, Claude J, Strimmer K. 2004. APE: Analyses of phylogenetics and evolution in R language. *Bioinformatics* 20: 289–290.
Páramo-Fonseca ME, Benavides-Cabra CD, Gutiérrez IE. 2018. A new large pliosaurid from the barremian (Lower Cretaceous) of Sáchica, Boyacá, Colombia. *Earth Sciences Research Journal* 22: 223–238.
Páramo-Fonseca ME, Benavides-Cabra CD, Gutiérrez IE. 2019. A new specimen of *Stenorhynchosaurus munozi* Páramo-Fonseca et al., 2016 (Plesiosauria, Pliosauridae), from the Barremian of Colombia: new morphological features and ontogenetic implications. *Journal of Vertebrate Paleontology* 39: 1–16.
Páramo-Fonseca ME, Gómez-Pérez M, Noè LF, Etayo-serna F. 2016. Stenorhynchosaurus munozi, gen. et sp. nov. a new pliosaurid from the Upper Barremian (Lower Cretaceous) of Villa de Leiva, Colombia, South America. *Revista de la Academia Colombiana de Ciencias Exactas, Físicas y Naturales* 40: 84–103.
R Core Team. 2016. R: A language and environment for statistical computing.
Romer AS, Lewis AD. 1959. A mounted skeleton of the giant plesiosaur *Kronosaurus*. *Breviora* 112: 1–15.
Ronquist F, Klopfstein S, Vilhelmsen L, Schulmeister S, Murray DL, Rasnitsyn AP. 2012. A total-evidence approach to dating with fossils, applied to the early radiation of the hymenoptera. *Systematic Biology* 61: 973–999.
Rothausen K. 1968. Die systematische stellung der europäischen Squalodontidae (Odontoceti, Mamm.). *Paläontologische Zeitschrift* 42: 83–104.
Sachs S, Hornung JJ, Kear BP. 2016. Reappraisal of Europe's most complete Early Cretaceous plesiosaurian: *Brancasaurus brancai* Wegner, 1914 from the "Wealden facies" of Germany. *PeerJ* 4: e2813.
Sassoon J, Foffa D, Marek R. 2015. Dental ontogeny and replacement in Pliosauridae. *Royal Society Open Science* 2: 150384.
Sassoon J, Noè LF, Benton MJ. 2012. Cranial anatomy, taxonomic implications and palaeopathology of an Upper Jurassic pliosaur (Reptilia: Sauropterygia) from Westbury, Wiltshire, UK. *Palaeontology* 55: 743–773.
Sato T. 2005. A new polycotylid plesiosaur (Reptilia: Sauropterygia) from the Upper Cretaceous Bearpaw Formation in Saskatchewan, Canada. *Journal of Paleontology* 79: 969–980.
Sato T, Wu XC, Tirabasso A, Bloskie P. 2011. Braincase of a polycotylid plesiosaur (Reptilia: Sauropterygia) from the Upper Cretaceous of Manitoba, Canada. *Journal of Vertebrate Paleontology* 31: 313–329.

Schumacher BA. 2007. A new polycotylid plesiosaur (Reptilia; Sauropterygia) from the Greenhorn Limestone (Upper Cretaceous; lower upper Cenomanian), Black Hills, South Dakota. *Geological Society of America Special Papers* 427: 133–146.
Schumacher BA. 2011. A 'woollgari-zone mosasaur' (Squamata; Mosasauridae) from the Carlile Shale (Lower Middle Turonian) of central Kansas and the stratigraphic overlap of early mosasaurs and pliosaurid plesiosaurs. *Transactions of the Kansas Academy of Science* 114: 1–14.
Schumacher BA, Carpenter K, Everhart MJ. 2013. A new Cretaceous Pliosaurid (Reptilia, Plesiosauria) from the Carlile Shale (middle Turonian) of Russell County, Kansas. *Journal of Vertebrate Paleontology* 33: 613–628.
Schumacher BA, Everhart MJ. 2005. A stratigraphic and taxonomic review of plesiosaurs from the old 'Fort Benton Group' of central Kansas: a new assessment of old records. *Paludicola* 5: 33–54.
Schumacher BA, Martin JE. 2015. *Polycotylus latipinnis* Cope (Plesiosauria, Polycotylidae), a nearly complete skeleton from the Niobrara Formation (Early Campanian) of southwestern South Dakota. *Journal of Vertebrate Paleontology*: e1031341.
Seeley HG. 1869. *Index of the fossil remains of Aves, Ornithosauria and Reptilia, from the Secondary System of Strata Aranged in the Woodward Museum of the University of Cambridge* (B Deighton, Ed.). Cambridge.
Seeley HG. 1874. Note on some of the generic modifications of the plesiosaurian pectoral arch. *Quarterly Journal of the Geological Society* 30: 436–449.
Smith MR. 2019. Bayesian and parsimony approaches reconstruct informative trees from simulated morphological datasets. *Biology Letters* 15: 20180632.
Smith AS, Dyke GJ. 2008. The skull of the giant predatory pliosaur *Rhomaleosaurus cramptoni*: implications for plesiosaur phylogenetics. *Naturwissenschaften* 95: 975–980.
Storrs GW, Taylor MA. 1996. Cranial anatomy of a new plesiosaur genus from the lowermost Lias (Rhaetian/Hettangian) of Street, Somerset, England. *Journal of Vertebrate Paleontology* 16: 403–420.
Tarlo LB. 1957. The scapula of *Pliosaurus macromerus* Philips. *Palaeontology* 1: 193–199.
Tarlo LB. 1959a. *Pliosaurus brachyspondylus* (Owen) from the Kimmeridge Clay. *Palaeontology* 1: 283–291.
Tarlo LB. 1959b. *Stretosaurus* gen. nov., a giant pliosaur from the Kimmeridge Caly. *Palaeontology* 2: 39–55.
Tarlo LB. 1960. A review of the Upper Jurassic pliosaurs. *Bulletin of the British Museum (Natural History) Geology* 4: 145–189.
Taylor MA, Cruickshank ARI. 1993. Cranial Anatomy and Functional Morphology of *Pliosaurus brachyspondylus* (Reptilia: Plesiosauria) from the Upper Jurassic of Westbury, Wiltshire. *Philosophical Transactions of the Royal Society B: Biological Sciences* 341: 399–418.
Tutin SL, Butler RJ. 2017. The completeness of the fossil record of plesiosaurs, marine reptiles from the Mesozoic. *Acta Palaeontologica Polonica* 62: 563–573.

VanBuren CS, Evans DC. 2016. Evolution and function of anterior cervical vertebral fusion in tetrapods. *Biological reviews of the Cambridge Philosophical Society*.
Wegner T. 1914. *Brancasaurus brancai* n. g. n. sp., ein Elasmosauride aus dem Wealden Westfalens. In: Scheondorf F, ed. *Branca-Festschrift*. Berlin: Bornträger, 235–305.
Welles SP. 1962. A new species of elasmosaur from the Aptian of Colombia, and a review of the Cretaceous plesiosaurs. *University of California Publications in Geological Sciences* 44: 1–96.
White TE. 1935. On the skull of *Kronosaurus queenslandicus* Longman. *Occasional papers of the Boston Society of Natural Hi* 8: 219–228.
White TE. 1940. Holotype of *Plesiosaurus longirostris* Blake and classification of the plesiosaurs. *Journal of Paleontology* 14: 451–467.
Williston SW. 1907. The skull of *Brachauchenius*, with observations on the relationships of the plesiosaurs. *Proceedings of the US National Museum* 32: 477–489.
Williston SW. 1925. *The osteology of the reptiles*. Cambridge, Massachusetts: Harvard University Press,.
Wintrich T, Hayashi S, Houssaye A, Nakajima Y, Sander PM. 2017. A Triassic plesiosaurian skeleton and bone histology inform on evolution of a unique body plan. *Science Advances* 3: e1701144.
Zammit M, Kear BP. 2011. Healed bite marks on a Cretaceous ichthyosaur. *Acta Palaeontologica Polonica* 56: 859–863.
Zverkov NG, Fischer V, Madzia D, Benson RBJ. 2018. Increased Pliosaurid Dental Disparity Across the Jurassic – Cretaceous Transition. *Palaeontology* 61: 825–846.
Zverkov NG, Pervushov EM. 2020. A gigantic pliosaurid from the Cenomanian (Upper Cretaceous) of the Volga Region, Russia. *Cretaceous Research* 110: 104419.

SUPPLEMENTARY INFORMATION

Anatomy and relationships of the bizarre Early Cretaceous pliosaurid *Luskhan itilensis*

Valentin Fischer[1,*], Roger B. J. Benson[2], Nikolay G. Zverkov[3], Maxim S. Arkhangelsky[4,5], Ilya M. Stenshin[6], Gleb N. Uspensky[7], Natalya E. Prilepskaya[8]

[1]Evolution & Diversity Dynamics Lab, Université de Liège, 14 Allée du 6 Août, Liège 4000, Belgium.
[2]Department of Earth Sciences, University of Oxford, South Parks Road, Oxford OX1 3AN, UK.
[3]Geological Institute of the Russian Academy of Sciences, Pyzhevsky Lane 7, Moscow 119017, Russia.
[4]Department of General Geology and Minerals, Saratov State University, A83 Astrakhanskaya Street, 410012 Saratov, Russia.
[5]Department of Geoecology and Engineering Geology, Saratov State Technical University, 77 Politekhnicheskaya Street, 410054 Saratov, Russia.
[6]Undory Paleontological Museum, Shkol'naya Ulitsa, 5, Undory, Ulyanovsk Oblast, 433340, Russia.
[7]Natural Science Museum, Ulyanovsk State University, Leo Tolstoy Street, Ulyanovsk 432000, Russia.
[8]Severtsov Institute of Ecology and Evolution of the Russian Academy of Sciences, 34 Vavilova Street, Moscow 119334, Russia.

*corresponding author: v.fischer@uliege.be

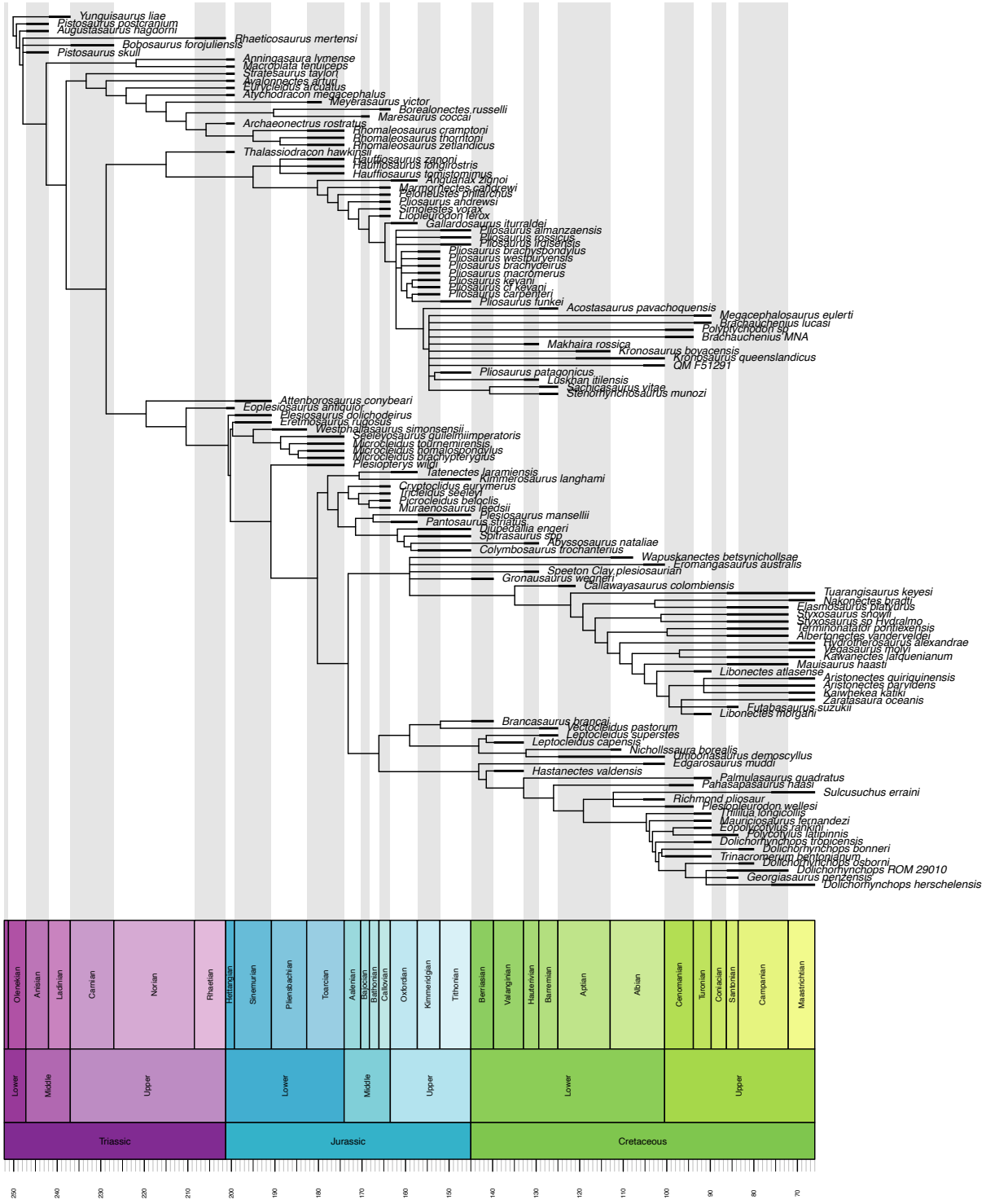

Figure S1. Phylogenetic relationships of Plesiosauria. Strict consensus, implied weighting, maximum parsimony (k=6).

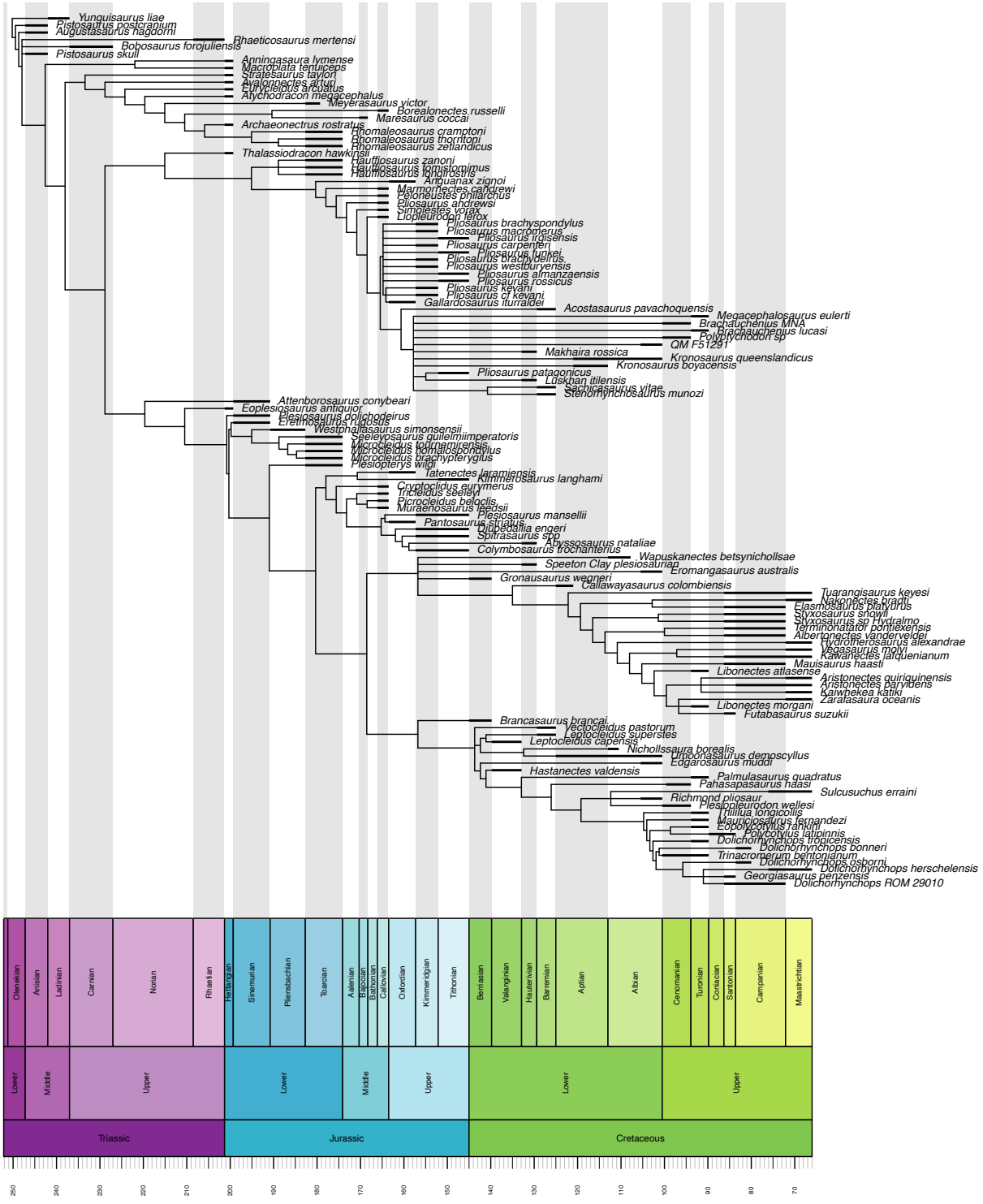

Figure S2. Phylogenetic relationships of Plesiosauria. Strict consensus, implied weighting, maximum parsimony (k=9).

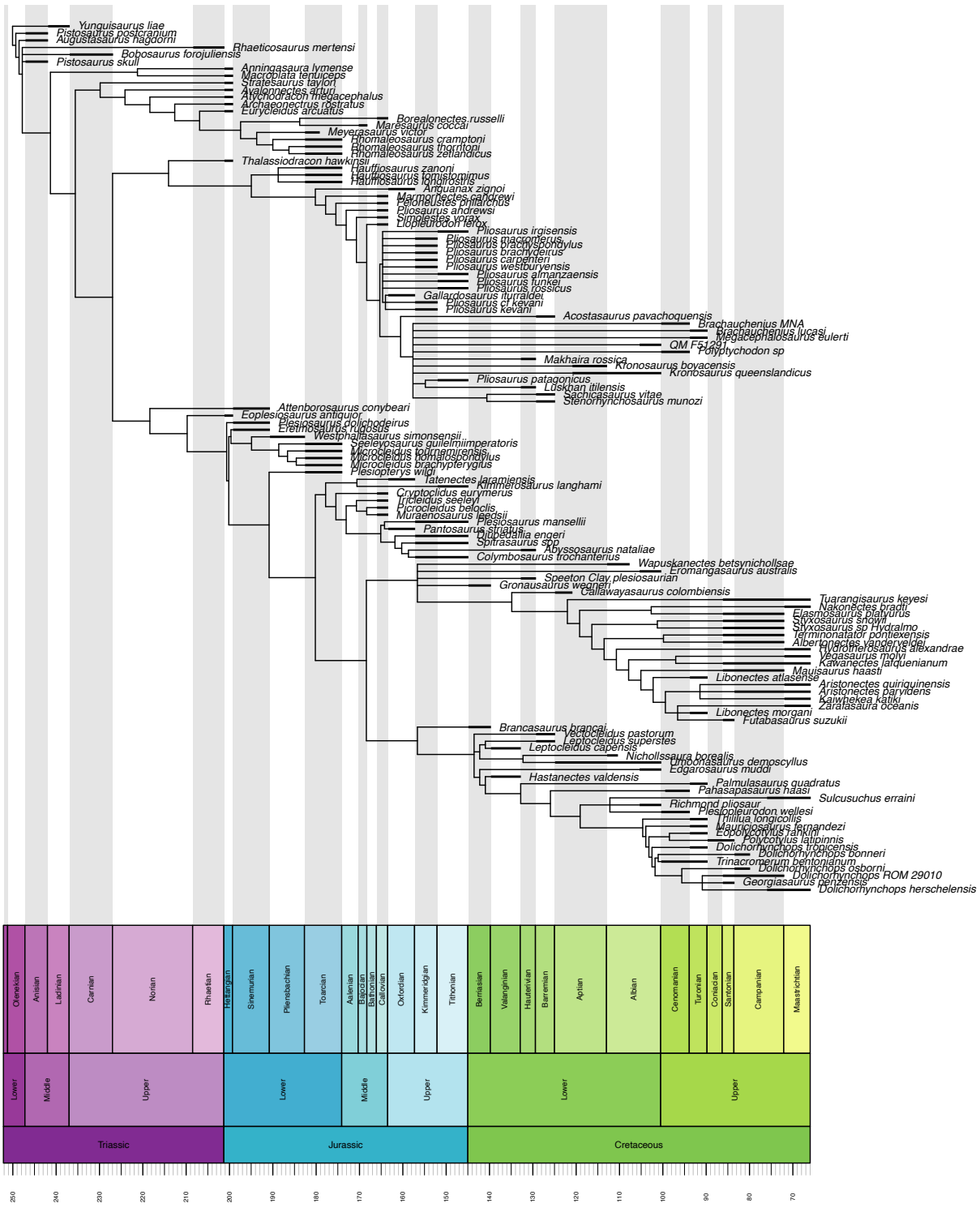

Figure S3. Phylogenetic relationships of Plesiosauria. Strict consensus, implied weighting, maximum parsimony (k=12).

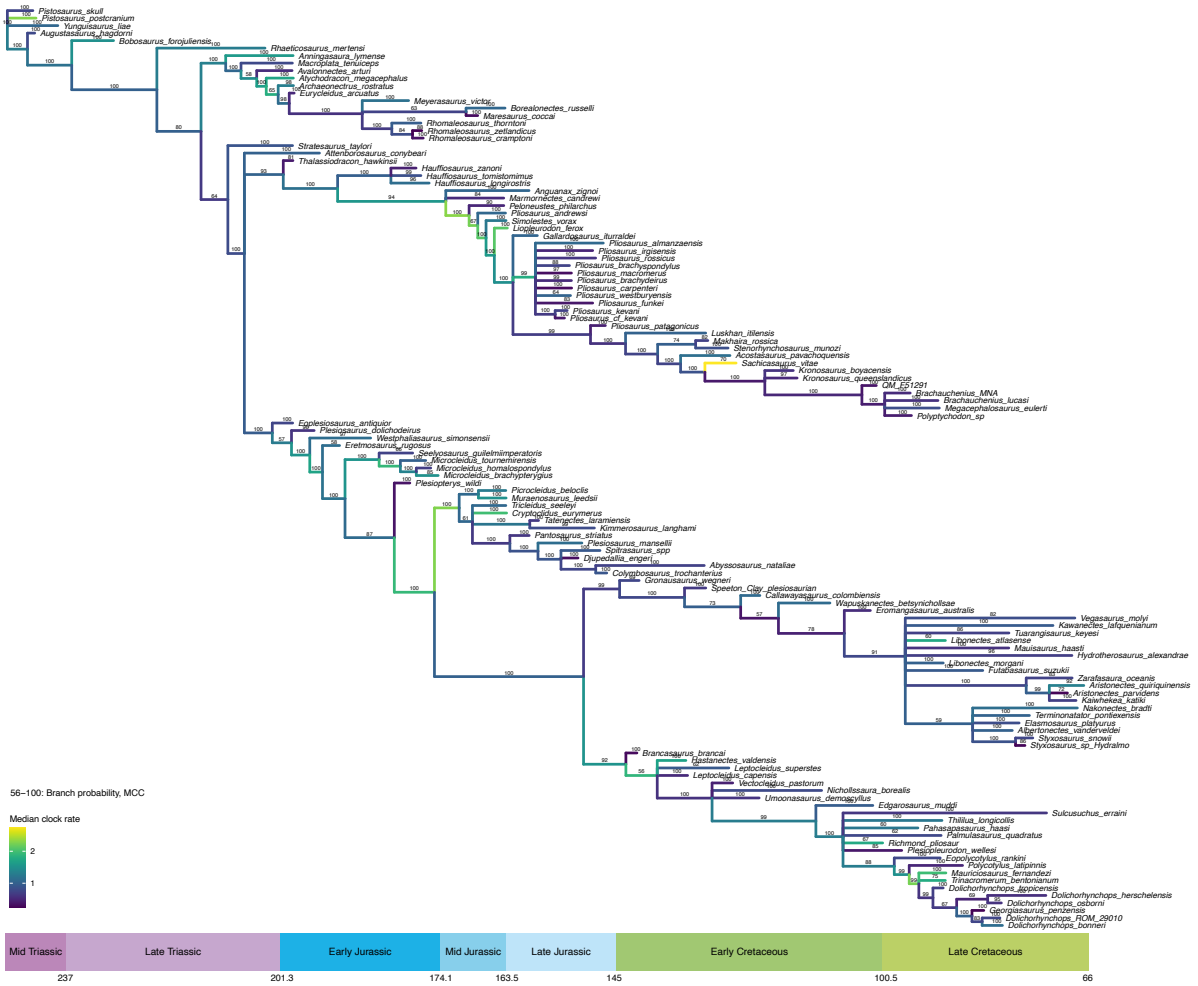

Figure S4. Phylogenetic relationships of Plesiosauria arising from the relaxed morphoclock Bayesian inference. “Allcompat” majority rule consensus.